

The Kinematic Properties of BHB and RR Lyrae stars towards the Anticentre and the North Galactic Pole: The Transition between the Inner and the Outer Halo.

T.D. Kinman^{1*}, C. Cacciari², A. Bragaglia², R. Smart³, A. Spagna³

¹ *NOAO, P.O. Box 26732, Tucson, AZ 85726-6732, USA*†

² *INAF, Osservatorio Astronomico di Bologna, Via Ranzani 1, I-40127 Bologna, Italy*

³ *INAF, Osservatorio Astronomico di Torino, Via Osservatorio 20, I-10025 Pino Torinese, Italy*

Accepted 2012 February 14. Received 2012 February 8; in original form 2011 November 29.

ABSTRACT

We identify 51 blue horizontal branch (BHB) stars, 12 possible BHB stars and 58 RR Lyrae stars in Anticentre fields. Their selection does not depend on their kinematics. Light curves and ephemerides are given for 7 previously unknown RR Lyrae stars. All but 4 of the RR Lyrae stars are of Oosterhoff type I.

Our selection criteria for BHB stars give results that agree with those used by Smith et al. (2010) and Ruhland et al. (2011). We use 5 methods to determine distances for the BHB stars and 3 methods for the RR Lyrae stars to get distances on a uniform scale. Absolute proper motions (largely derived from the GSCII and SDSS (DR7) databases) are given for these stars; radial velocities are given for 31 of the BHB stars and 37 of the RR Lyrae stars.

Combining these data for BHB and RR Lyrae stars with those previously found in fields at the North Galactic Pole, we find that retrograde orbits dominate for galactocentric distances greater than 12.5 kpc. The majority of metal-poor stars in the solar neighbourhood are known to be concentrated in a L_{\perp} vs. L_z angular momentum plot. We show that the ratio of the number of *outliers* to the number in the *main concentration* increases with galactocentric distance. The location of these *outliers* with L_{\perp} and L_z shows that the halo BHB and RR Lyrae stars have more retrograde orbits and a more spherical distribution with increasing galactocentric distance. Six RR Lyrae stars are identified in the H99 group of *outliers*; the small spread in their [Fe/H] suggests that they could have come from a single globular cluster. Another group of *outliers* contains two pairs of RR Lyrae stars; the stars in each pair have similar properties.

Key words: Stars: kinematics; Stars: horizontal branch; Stars: variables: RR Lyrae; Galaxy: structure; Galaxy: halo

1 INTRODUCTION

The blue horizontal branch (BHB) and RR Lyrae stars are well-established tracers of the oldest stars in the galactic halo although their galactic distribution may not coincide with other halo tracers such as the turn-off stars (Bell et al. 2010). This paper continues those on other surveys for BHB and RR Lyrae stars (Kinman et al. 2007b and Kinman & Brown 2011) and extends previous work in the Anticentre direction (Kinman et al. 1994). Our BHB and RR Lyrae stars are in the range $10 < V < 17$ and so range in distance

from those in the solar neighbourhood to those distant enough to be included in the SDSS DR 7 survey (Abazajian et al. 2009). This allows our selection methods for BHB stars to be compared with other methods for identifying halo SDSS stars (Smith et al. 2010 and Ruhland et al. 2011).

The globular-cluster halo is thought to consist of an Old Halo and a Young Halo in which the clusters have different horizontal branch (HB) morphologies that can be interpreted as an age difference (Zinn 1993). The shape of the field star halo changes with galactocentric distance (Schmidt 1956; Kinman et al. 1966) which suggests that it may not be homogeneous. It is now usual to postulate that the field stars belong to an “inner halo” that was formed *in situ* and an “outer halo” that has largely been accreted. Earlier work on the field star halo has been summarized by Helmi (2008).

* e-mail: kinman@noao.edu

† NOAO is operated by AURA Inc. under contract with the National Science Foundation.

Since then, there have been several more investigations of halo structure using various tracers. Surveys using BHB stars have been made by Smith et al. (2010), Xue et al. (2011), Ruhland et al. (2011) and Deason et al. (2011). Surveys using RR Lyrae stars have been made by Watkins et al. (2009), and Sesar et al. (2010). The stars in these surveys are mostly too distant to have good proper motions from which space motions could be derived. They do, however, allow space densities to be determined as a function of galactocentric distance. The surveys of Deason et al. (2011) for BHB stars and of Sesar et al. (2011) for turn-off stars both show breaks in the slopes of their density distributions at 28 kpc from the galactic centre; this suggests that the halo may have two components.

Recent surveys for stars that are close enough for existing proper motions to allow a kinematic analysis include the survey for subdwarfs by Smith et al. (2009), but this survey does not extend far enough in galactocentric distance to sample the outer halo. Carollo et al. (2007, 2010) have analyzed the space motions of a large number of stars within 4 kpc and find that a two-component halo is needed to account for the galactic rotation of these stars. They find that there is an outer halo that is more metal-poor and that has a more retrograde rotation than the inner halo. It should be noted that two halos overlap spatially and the outer halo is less centrally concentrated than the inner. The difference in metallicity between the two halos has been confirmed by De Jong et al. (2010). Recently Carollo et al. (2012) have shown that the fraction of carbon-enhanced metal-poor stars is twice as great in the outer halo as in the inner halo. Schönrich, Asplund & Casagrande (2011) re-analysed the Carollo et al. (2010) data and failed to find any reliable evidence for an outer counter-rotating halo. Inter-alia they criticized the luminosity classification of the turn-off stars. In a rebuttal, Beers et al. (2012) re-analyzed their data (re-classifying the turn-off stars and criticizing the main-sequence luminosity relation used by Schönrich et al.); they substantiate their original conclusion that the inner halo is nearly non-rotating while the outer halo has “a retrograde signature” with a transition at 15 to 20 kpc from the Sun.

Recent simulations of galaxy formation support the idea that the halos of galaxies like the Milky Way have a dual origin and have been formed both in-situ and by accretion (Zolotov et al., 2009, 2010, 2011), (Oser et al., 2010). (Font et al., 2011), (McCarthy et al., 2012). Zolotov (2011) discusses a dual halo in which the role of accretion increases outwards from the Galactic centre and the halo is formed solely by accretion if $R_{gal} > 20$ kpc. In these simulations, the fraction of the halo that is accreted depends upon the mass of the galaxy. The average of the 400 simulations given by Font et al. has the inner “in situ” component dropping to 20% and the accreted component rising to 80% at a galactocentric distance of 20 kpc. McCarthy et al. (2012) find that the “in situ” component has a flattened distribution and a rotation that is intermediate between that of the disc and the “outer halo”.

In this paper we examine halo stars in the Anticentre direction because this is the best direction in which to study the transition from the “in situ” to the accreted halo and the kinematic properties of the outer halo. We do not have sufficient data to discuss the abundance differences between the two halos. Sec. 2 identifies the sources and their galactic distributions from which our BHB candidates and our RR Lyrae stars are taken. In Sec. 3 we give the photometric data for the BHB stars and in Appendix A we describe the techniques used to identify these stars and the methods used to estimate their distances. Sec. 4 gives the photometric data and periods for the RR Lyrae stars and shows that they mostly belong to Oosterhoff type 1; in Appendix B we give the ephemerides for the new RR

Lyrae stars and the methods used to estimate their distances. Sec. 5 gives the adopted distances, proper motions and radial velocities of our program stars together with their galactic space motions. It is shown in Sec. 5 that the galactic rotation velocity (V) becomes more retrograde with increasing galactocentric distance. Appendix C gives details of the sources of the proper motions. Sec.6 introduces the angular momenta L_z and L_{\perp} and their relation to the galactic rotation (V) and the maximum height above the plane of the star’s orbit (Z_{max}). It is shown the halo becomes more spherical with increasing galactocentric distance. Appendix D discusses the location of thick disc in the L_z and L_{\perp} plot. Appendix E gives the angular momenta of the RR Lyrae and BHB stars near the North Galactic Pole, those of the local BHB stars and those of the galactic globular clusters within 10 kpc. Appendix F discusses the properties of the kinematic groups H99 and K07. The results of the paper are summarized in Sec. 7.

2 TARGET SELECTION

Our study of the Anticentre halo began with a search for RR Lyrae stars in the fields RR VI ($l = 180^\circ$, $b = +26^\circ$) and RR VII ($l = 183^\circ$, $b = +37^\circ$); each field covers an area of 30 deg^2 (Kinman et al. 1982). Later Sanduleak provided BHB star candidates for the RR VII field and these were discussed by Kinman et al. (1994). These samples of BHB and RR Lyrae stars have been enlarged for the present paper. New BHB candidates were taken from the objective prism surveys of Pesch & Sanduleak (1989; Case A-F stars) and of Beers et al. (1996; BPS BS stars). We are indebted to Dr Peter Pesch (1996, private communication) for sending us unpublished candidate stars from the Case survey. These are given the prefix P in column 2 of Table 4 unless there is a previous identification in the literature.

Our methods of selecting BHB stars from these candidates and the calculation of their distances are described in Appendix A. Apart from the RR Lyrae stars in fields RR VI and RR VII, the additional RR Lyrae stars have mostly been found among BHB candidates that were found to be variable. Seven of these RR Lyrae stars have not been previously identified and their light curves and ephemerides are given in Appendix B. All our program stars are listed in Tables 4 and 5 for the BHB and RR Lyrae stars respectively. These tables give positions and photometric data for the BHB stars and, also, metallicities and periods for the RR Lyrae stars; sources of these data are given in notes to these tables.

The galactic distributions of our program stars are shown separately for the BHB and RR Lyrae stars in Fig. 1. Not only do our BHB and RR Lyrae stars cover somewhat different areas of the Anticentre sky, but they also cover different magnitude ranges so that the volumes of space that they occupy only partially overlap. Also, our selection of RR Lyrae stars favours the bluer (Bailey type *c*) and may miss some of the redder (Bailey type *ab*) RR Lyrae variables and so our sample may not be complete. This must be taken into account in comparing the properties of our two samples.

The period-amplitude distribution of our RR Lyrae sample is shown in Fig. 2 for the variables with galactic latitudes less than 50° . The solid and dotted curves show the loci of the Oosterhoff type I and II variables respectively (these were taken from Cacciari et al. 2005). Most of our RR Lyrae stars lie close and to the left of the Oo I curve; this suggests that the majority are Oo I variables. The four stars that are most likely to be Oo II variables are indicated by their numbers in Fig. 2. This preponderance of Oo I variables in the Anticenter is compatible with the discovery by Miceli et al.

(2008) that the Oo II variables are more concentrated towards the Galactic centre than the Oo I variables. The ratio of Oo I to Oo II variables should therefore increase with galactocentric distance and so the Oo I variables should predominate towards the Anticentre.

3 THE BHB STARS.

Our BHB stars were chosen from *candidates* in the sources given in Section 2. Table 4 gives the equatorial and galactic coordinates of these stars, together with photometric data (using the system used in Kinman et al. 1994). Details of the photometric observing are given in Kinman et al. (1994) for photoelectric observations and Kinman & Brown (2011) for CCD observations. Table 4 also gives the *GALEX NUV* magnitude (effective wavelength 2267 Å) that was taken from *MAST*.¹ We assumed that stars with $V < 12.5$ had saturated *GALEX NUV* magnitudes and should not be used. We also give the *2MASS K* magnitude that was taken from the *2MASS* Point Source Catalog using the *Vizier* access tool.

The selection of BHB stars from the candidates is described in Appendix A. We show there how a weight W (Table 4, column 13) was assigned to each star that depends on the probability that it is a BHB star. The stars were given a type (Table 4, column 15) that depended on this weight. Stars with a high probability of being BHB stars were classified as *BHB*, those with a high probability of not being BHB were classified as *A* while intermediate types were classified as *bhb*. A comparison of our classifications with those obtained by methods based on SDSS photometry suggests that stars with both *BHB* and *bhb* classifications have a high probability of being BHB stars.

Appendix A also contains a discussion of five different methods of getting the absolute magnitudes (and hence distances) of BHB stars. These distances and the adopted distances are given in Table A1. The reddenings of both BHB stars and RR Lyrae stars were taken from Schlegel et al. (1998).

4 THE RR LYRAE STARS.

Most of the RR Lyrae stars in Table 5 are listed in the General Catalogue of Variable Stars (GCVS, Kholopov et al., 1985) and subsequent Name Lists and have the traditional identification by constellation; those without GCVS names are taken from Pier et al. (2003), Kinman et al. (2004) and Kinman & Brown (2010). Seven of the stars in Table 5 have not been previously identified as RR Lyrae stars; their light curves and ephemerides are given in Appendix B. The mean K magnitudes ($\langle K \rangle$) in Table 5 were derived from the *2MASS K* magnitudes using the method given in Feast et al. (2008). We follow the methods given in Kinman et al. (2007b) to derive distances for the RR Lyraes. These are briefly restated in Appendix B where we give distances by three separate methods together with adopted distances (D) that are adjusted to be on the same scale as those adopted for the BHB stars (Appendix A).

4.1 Oosterhoff types of the RR Lyrae stars.

The globular clusters with Oosterhoff type I RR Lyrae stars are known to have different kinematics (more retrograde orbits) than those containing Oosterhoff type II RR Lyrae stars (Lee & Carney,

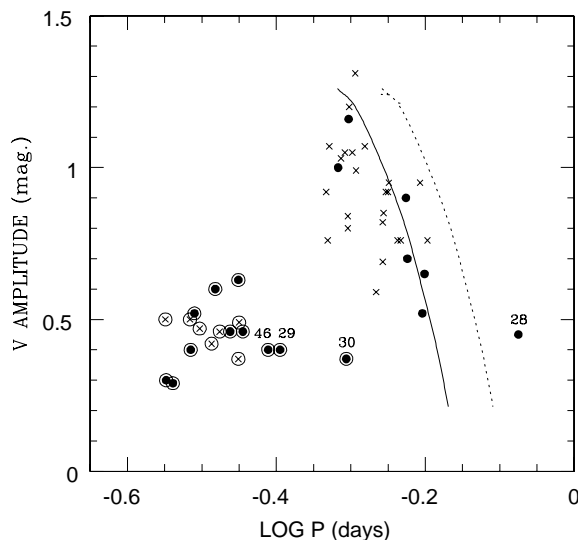


Figure 2. The V amplitude vs. log Period plot for our RR Lyrae sample with galactic latitudes less than 50° . Filled circles indicate stars for which a V amplitude was available. Crosses indicate stars where the V amplitude was obtained by dividing the B amplitude by 1.31. Encircled filled circles and crosses show Bailey type c variables. The solid and dotted curves show the expected loci for Oo type I and Oo II variables of Bailey type ab respectively and were taken from Cacciari et al. (2005). The four likely Oo II variables are given their numbers in Table 5.

1999; van den Bergh 1993).² The Oosterhoff type is determined from the period-amplitude diagram and this is shown in Fig. 2 for our RR Lyrae sample with $b \leq 50^\circ$. In this figure the loci for the Oosterhoff type I and II variables are shown by solid and dotted curves respectively (these curves were taken from Cacciari et al. 2005). Most of our RR Lyrae stars lie close and to the left of the Oo I curve. Type ab stars that lie to the left of the Oo I curve may either be metal-rich or have smaller mean amplitudes because of Blazhko effect. This suggests that the majority of our stars are Oo I variables. Four stars that are most likely to be Oo II variables are indicated by their numbers in Fig. 2. Stars 29, 30 and 46 are type c variables while 28 is type ab . These four stars have $\langle Z \rangle = 3.9$ kpc and $\langle R_{gal} \rangle = 14.3$ kpc compared with $\langle Z \rangle = 6.6$ kpc and $\langle R_{gal} \rangle = 19.6$ kpc for the whole sample. The preponderance of Oo I variables in our Anticenter fields and the smaller $\langle R_{gal} \rangle$ of our Oo II variables is to be expected if the Oo II variables are more concentrated towards the Galactic centre than the Oo I variables (Miceli et al. 2008). The smaller $\langle Z \rangle$ of our Oo II variables also agrees with the preponderance of Oo I variables at high Z that was found by De Lee (2008). This suggests that the Oo II variables are not only more concentrated to the Galactic centre but also form a more flattened system than the Oo I variables.

¹ The Multimission Archive at the STScI, <http://archive.stsci.edu/>.

² The simple division into two Oosterhoff types does not cover all cases (Smith et al. 2011) but is a good approximation for our own Galaxy.

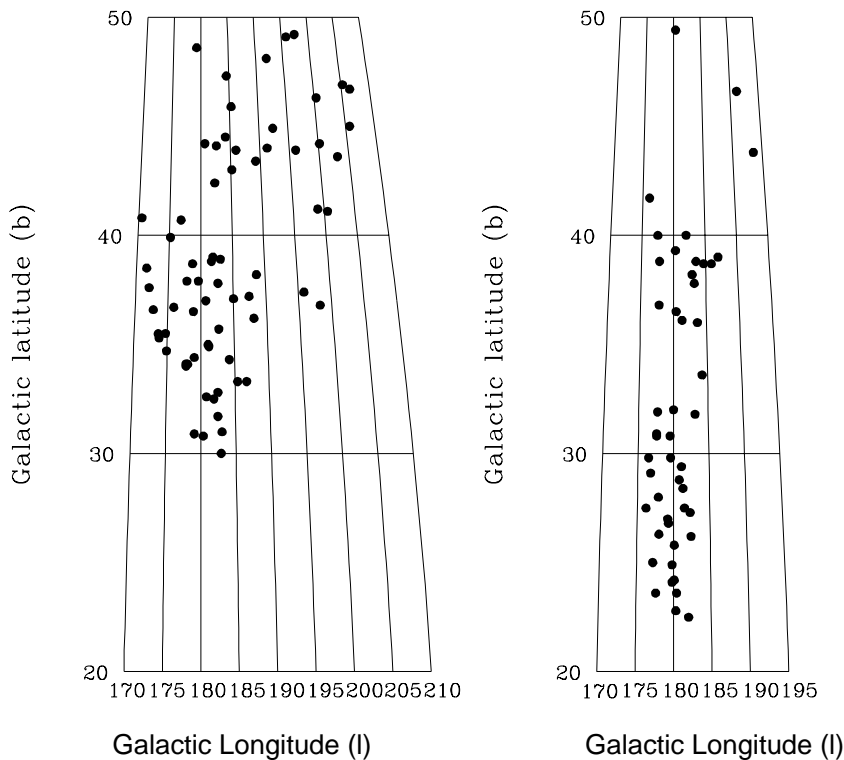


Figure 1. The distribution in galactic coordinates (expressed in degrees) of (left) the BHB candidates from Table 4 and, (right) our program RR Lyrae stars (Table 5). Seven RR Lyrae stars with $b > 50^\circ$ are omitted from this Figure.

5 THE GALACTIC SPACE MOTIONS OF THE PROGRAM STARS.

Tables 6 and 7 give the parallaxes, proper motions, radial velocities and the Galactic Space Motions (U,V,W) with respect to the Local Standard of Rest (LSR) for the BHB and bhb stars and the RR Lyrae stars respectively. The parallaxes are derived from the adopted distances (D) given in Tables A1 and B2 in Appendices A and B respectively. The error in the parallax is derived from the rms scatter given in the last columns of Tables A1 and B2 and does not include any systematic error in the case of the BHB stars. In the case of the RR Lyrae stars, a small distance-dependent error has been added in quadrature to the rms scatter to derive the error of the parallax as explained in the appendix Sec. B2. Heliocentric space-velocity components U, V, and W were derived from the data listed in these tables. We used the program by Johnson & Soderblom (1987) (updated for the J2000 reference frame and further updated with the transformation matrix derived from the Vol. 1 of the Hipparcos data catalogue). This program gives a right-handed system for U, V and W in which these vectors are positive towards the directions of the Galactic centre, but we here use the left-handed system so as to be comparable with most other recent work. These heliocentric velocities were then corrected to velocities relative to the LSR using the solar motion relative to the LSR $(U, V, W)_\odot = (10.0, 5.25, 7.17) \text{ km s}^{-1}$ (Dehnen & Binney 1998).

5.1 Radial velocities and Proper Motions

The sources of our radial velocities are given in column (8) (S_{RV}) of Tables 6 and 7. The Bologna velocities were derived from spectra taken with the 3.5m-LRS (TNG) spectrograph. The Kitt Peak velocities were derived from spectra taken with RC spectrograph on the 4m Kitt Peak telescope and kindly made available to us by Nick Suntzeff (1997, private communication). The remaining velocities were taken from the literature as given in the notes to Tables 6 and 7.

The absolute proper motions given in this paper come primarily from astrometric data assembled from the Second Guide Star Catalog (GSC-II; Lasker et al. 2008), and the Seventh Data Release of the Sloan Digital Sky Survey (SDSS DR7; Abazajian et al. 2009; Yanny et al. 2009). Details are given in Appendix C. In the case of a few of the brighter stars ($V < 12.3$) we have chosen the proper motions given in the NOMAD Catalog (Zacharias et al. 2004). In the case of the BHB star P 30-38, we chose the proper motion given by the SDSS DR7 because the GSC-II—SDSS proper motion has unusually large errors. The SDSS DR7 proper motions have also been used for the stars (mostly BHB stars) for which GSC-II—SDSS proper motions were not available.

We have only used stars that have radial velocities to compute U, V and W, and since only 4 of the BHB stars that only have SDSS DR7 proper motions also have radial velocities, possible systematic differences between the SDSS DR7 and the GSC-II—SDSS proper motions should have little effect on our overall results³. A com-

³ In our discussion of halo stars at the North Galactic Pole (Kinman et

parison of the SDSS DR7 and the GSC-II—SDSS proper motions (Appendix C) shows good agreement at the 1 mas y^{-1} level; this corresponds to a tangential velocity of 40 km s^{-1} at a distance of 8.5 kpc.

5.2 Discussion of the space motions U, V & W

Table 1 gives the space motions for various subgroups of our program stars; all velocities are with respect to the LSR. The possible BHB stars (type bhb) have a V motion and velocity dispersions (σ_u , σ_v and σ_w) that are similar to those of the local BHB stars. This suggests that the majority are BHB stars but, conservatively, we have not included them in any of the other samples.

We have used the angular momenta (L_\perp and L_z) to distinguish between *disc* and *halo* stars. These quantities are defined in the Appendix of Kewley et al. (2007) and are given for our program stars in columns 15 and 16 of Tables 6 and 7. Following the discussion given in our Appendix D2, we identify the BHB star RR7 064 and the RR Lyrae stars TW Lyn and P 82 06 as probable *disc* stars and have excluded them from further discussion.

We assume that $\langle V \rangle = -V_{LSR} = -220 \text{ km s}^{-1}$ for zero halo rotation although higher values are possible⁴. We divide our program stars into samples according to distance: (A) those nearer than 8.5 kpc, and (B) those with distances between 8.5 and 17.0 kpc. At 17 kpc, an error of 1 mas in the proper motion will give an error of 80 km s^{-1} in the transverse velocity. With our relatively small samples, the inclusion of more distant stars would not add useful information. Our results are given in Table 1. The samples that contain an adequate number (N) of stars, namely BHB(A), RR (A) and RR (B), have mean U and W velocities that are essentially zero; this suggests that the systematic errors in our proper motions are not having a significant effect on the results for these samples. The velocity dispersions in Table 1 were corrected following Jones & Walker (1988); if the observed dispersion in U is $\text{Disp}(U)$, and ξ_i is the error in U of star i , then the corrected dispersion σ_u is given by:

$$\sigma_u^2 = (\text{Disp}(U))^2 - \frac{1}{n} \sum_{i=1}^n \xi_i^2$$

The corrected dispersions of U, V & W in our Anticentre samples are also comparable (within their errors) with those of the local samples.

Fig. 3(a), 3(b) and 3(c) are plots of the galactic velocity components $\langle V_{lsr} \rangle$, $\langle U_{lsr} \rangle$ and $\langle W_{lsr} \rangle$ respectively against galactocentric distance (R_{gal}) for both our Anticentre stars and those at the North Galactic Pole (Kinman et al. 2007b). Although there is considerable scatter between the different samples, there is clearly a trend in $\langle V_{lsr} \rangle$ from zero galactic rotation in the solar neighbourhood to a strong retrograde rotation for R_{gal} greater than 12.5 kpc. On the other hand, both $\langle U_{lsr} \rangle$ and $\langle W_{lsr} \rangle$ are essentially zero at all Galactocentric distances. This supports our conclusion that the

al. 2007b), the BHB and RR Lyrae stars were both closely grouped near the NGP and it seemed reasonable to adopt a zero radial velocity for stars whose radial velocity was not known in computing their galactic velocity V. This assumption has not been made for the more widely spread stars in the Anticentre.

⁴ e.g. $-236 \pm 15 \text{ km s}^{-1}$ (Reid & Brunthaler 2004); $-246 \pm 7 \text{ km s}^{-1}$ (Brunthaler et al. 2011).

trend of $\langle V_{lsr} \rangle$ with galactocentric distance is real and not produced by systematic errors in the proper motions. If the outer halo has a significantly retrograde rotation, as originally found by Carollo et al. (2007, 2010), and confirmed by Beers et al. (2012), this suggests that the outer halo dominates beyond $R_{gal} = 12.5 \text{ kpc}$.

6 STRUCTURE IN THE MOTIONS OF OUR HALO STARS.

Plots of the angular momenta L_\perp and L_z can be used to demonstrate kinematic structure among halo stars (e.g. Helmi et al. 1999). We give a L_\perp vs. L_z plot for our Anticentre BHB and RR Lyrae stars in Fig 4(a) and in Fig 4(b) for our North Galactic Pole sample of these stars (Kinman et al. 2007b). Similar plots are shown in Fig 5 for local RR Lyrae and BHB stars and in Fig 6 for the globular clusters within 10 kpc. Definitions of L_\perp and L_z are given by Kewley et al. (2007). We calculated these quantities and their errors with a program that was kindly made available by Heather Morrison and modified for our use by Carla Cacciari. The values of L_\perp and L_z for the North Galactic Pole RR Lyrae stars and BHB stars, the local BHB stars and the globular clusters within 10 kpc are tabulated in Appendix E, where we also compare our L_\perp and L_z with those calculated by Re Fiorentin et al. (2005) and Morrison et al. (2009) for a small sample of halo stars⁵.

L_z correlates with galactic rotation: in the left-handed system of coordinates, objects with positive L_z are prograde (the Sun has $L_z \sim 1760 \text{ kpc km s}^{-1}$) and those with negative L_z are retrograde. L_\perp correlates with the maximum height of the orbit above the plane (Fig. 7).

Morrison et al. (2009) investigated the L_\perp vs. L_z plot for 246 local metal-poor stars. The majority ($\sim 90\%$) of their sample, which we will call the *main concentration*, are in the location bounded by the black dotted line in Figs. 4, 5 & 6. This is taken from the outer contour of their Fig. 3. They also discovered a flattened component whose location is shown by the full black contour in our Figs. 4, 5 & 6. The remaining 10% of their sample lie outside the black dotted contour and, following Kewley et al. (2007) and Smith et al. (2009), we call them *outliers*. About a third of these *outliers* in the Morrison et al. (2009) sample belong to the prograde group (H99) discovered by Helmi et al. (1999) and further investigated by Re Fiorentin et al. (2005); its location of the majority of stars in this group is shown by the black rectangle in Figs 4, 5 & 6. The green rectangle shows the location of another group suggested by Kewley et al. (2007). The magenta box in Figs. 4, 5 & 6 shows the location of stars in the *main concentration* that have a high probability belonging to the Thick Disc; this is discussed in Appendix D.

The review by Klement (2010) lists sixteen halo “streams” that have been identified among stars in the solar neighbourhood. All except the H99 and Kapteyn Group lie within the *main concentration* in the L_\perp vs. L_z plot. An example of structure within the *main concentration* is shown by the RR Lyrae stars at distances between 1 and 2 kpc (Fig 5b) which are less evenly distributed than those at distances less than 1 kpc (Fig. 5a). In general, the identification of structure in this *main concentration* is only possible for stars with relatively large proper motions and well determined distances.

⁵ The data for the local RR Lyraes in Fig. 5 were either taken from Morrison et al. (2009) or calculated from the data given by Maintz & de Boer (2005); in this latter case no errors are given since Maintz & de Boer do not give errors for their data. The L_\perp and L_z for the globular clusters were calculated from data given in Table 3 of Vande Putte and Cropper (2009).

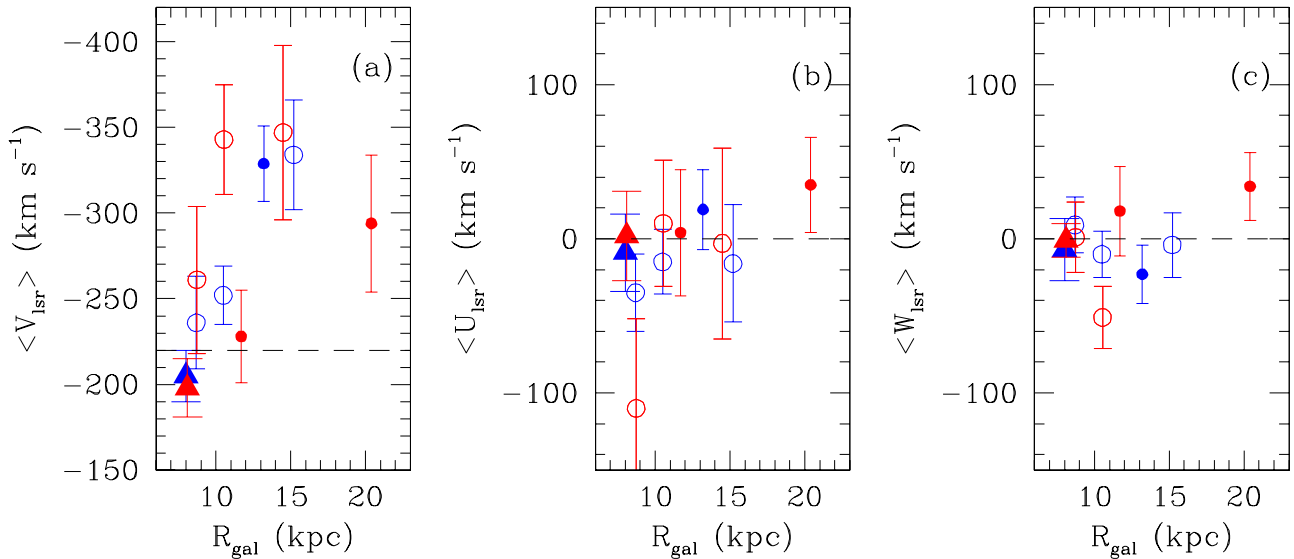


Figure 3. In (a) the ordinate is $\langle V_{lsr} \rangle$ in km s^{-1} . In (b) the ordinate is $\langle U_{lsr} \rangle$ in km s^{-1} . In (c) the ordinate is $\langle W_{lsr} \rangle$ in km s^{-1} . The abscissa is the Galactocentric distance in kpc. NGP BHB stars (blue open circles); NGP RR Lyrae stars (red open circles); Anticentre BHB stars (blue full circles); Anticentre RR Lyrae stars (red full circles); Local BHB stars (blue full triangles); Local RR Lyrae (red full triangles). It is seen that $\langle V_{lsr} \rangle$ becomes more retrograde while $\langle U_{lsr} \rangle$ and $\langle W_{lsr} \rangle$ remain unchanged with increasing Galactocentric distance.

Table 1. Space Motions U, V & W with respect to LSR and their dispersions σ_u, σ_v & σ_w in km s^{-1} .

Sample	N	U km s^{-1}	σ_u km s^{-1}	V km s^{-1}	σ_v km s^{-1}	W km s^{-1}	σ_w km s^{-1}	$\langle Z \rangle$ kpc	$\langle D \rangle$ kpc	$\langle R_{gal} \rangle$ kpc	Notes
bhb	8	-73 ± 41	115 ± 29	-192 ± 45	121 ± 30	-55 ± 48	134 ± 34	3.8	6.2	13.4	1
BHB (A)	28	$+19 \pm 26$	131 ± 18	-329 ± 21	99 ± 13	-14 ± 20	99 ± 13	3.7	6.1	13.2	2
RR (A)	15	$+3 \pm 40$	152 ± 28	-228 ± 26	95 ± 17	$+18 \pm 28$	108 ± 20	2.8	4.5	11.7	3
BHB (B)	3	-177 ± 69	89 ± 36	-181 ± 95	107 ± 44	$+86 \pm 98$	118 ± 48	6.0	9.8	16.9	4
RR (B)	16	$+31 \pm 29$	97 ± 17	-263 ± 40	121 ± 21	$+6 \pm 28$	78 ± 14	6.8	13.4	20.7	5
LOCAL BHB	27	$+9 \pm 25$	129 ± 18	-205 ± 15	79 ± 11	-7 ± 20	101 ± 14	8.0	6
LOCAL RR	32	-12 ± 29	160 ± 20	-204 ± 19	107 ± 13	$+11 \pm 20$	113 ± 14	8.0	7

Notes to Table:

- (1) Stars classified as bhb (possible BHB stars) (2) Halo BHB stars with $D < 8.5$ kpc. (3) Halo RR Lyrae stars with $D < 8.5$ kpc. (4) Halo BHB stars with $D > 8.5$ kpc. (5) Halo RR Lyrae stars with $8.5 < D < 17$ kpc. (6) Local sample of BHB stars (Kinman et al. (2007b)). (7) Local sample of Halo RR Lyrae stars within 1 kpc from Maintz & de Boer (2005). Velocity dispersions are upper limits. For further details see text.

In discussing our program stars, we shall therefore largely confine ourselves to discussing the *outliers* and the ratio of the number of *outliers* to the the number in the *main concentration*.

6.1 Ratio of the number of *outliers* to the number in the *main concentration*.

The ratio of the number of *outliers* to the number in the *main concentration* is a simple measure of the spread of halo stars in the L_{\perp} vs L_z plot. Our sample of globular clusters within 10 kpc contains 5 (with $[\text{Fe}/\text{H}] > -1.0$) that belong to the disc or bulge. Among the remainder, 24 belong to the main concentration and 2 (or 8%) are *outliers*. The two *outliers* are NGC 3201 and NGC 6205 (M13).

Although these two clusters are listed as “young” by Marín-Franch et al. (2009), Dotter et al. (2010) give ages of 12.00 ± 0.75 and 13.0 ± 0.50 Gyr for NGC 3201 and NGC 6205 respectively, which does not support this description. NGC 6205 (together with NGC 5466, NGC 6934 and NGC 7089) is one of a group of four globular clusters with similar L_{\perp} and L_z that are discussed by Smith et al. (2009) in connection with an overdensity in the subdwarfs that they studied. Smith et al. list the properties of 12 *outlier* subdwarfs that lie at heliocentric distances up to 5 kpc. They are shown by yellow open circles in Figs. 4(a) and (b). They show some tendency to occur in groups among themselves in their L_{\perp} vs L_z plot (as discussed by Smith et al.) but their locations in our plot (Figs. 4(a) and (b)) show little in common with those of our RR Lyrae and BHB *outliers*.

The local BHB stars within 1 kpc all belong to the *main concentration* and have no *outliers*. The RR Lyrae stars within 1 kpc

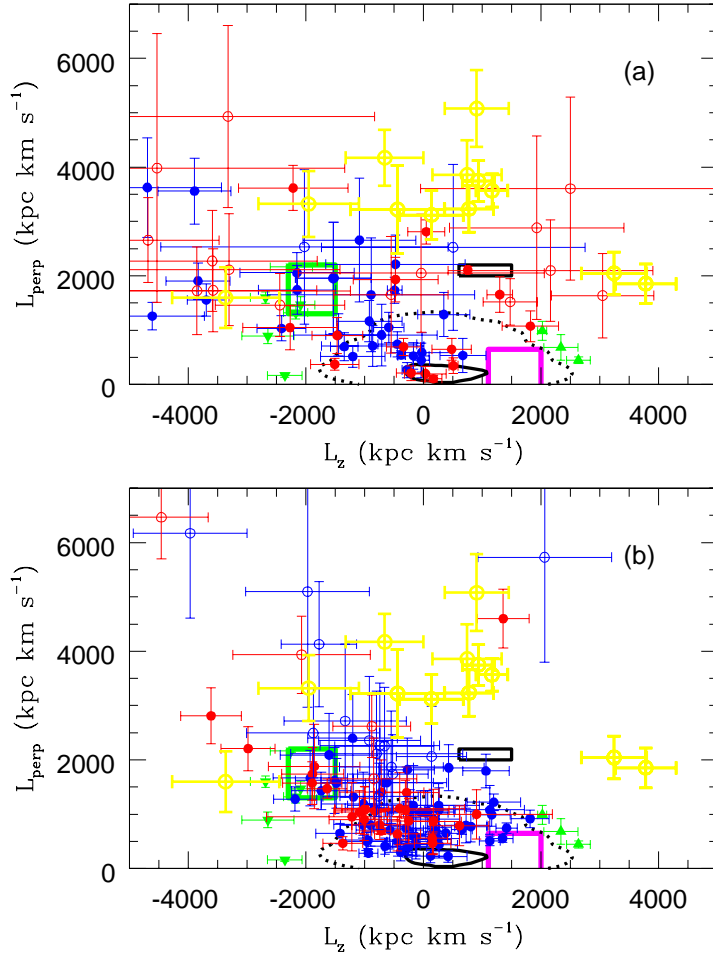


Figure 4. A plot of L_{\perp} against L_z for (a) stars in the Anticentre, and (b) stars at the North Galactic Pole. The black dotted curve is the outer contour of the majority of stars studied by Morrison et al. (2009); the black full curve is the flattened distribution that they discovered. The black and green rectangles are the locations of the groups discovered by Helmi et al. (1999) and Kepley et al. (2007) respectively. The magenta box shows the location of the Thick disc. BHB and RR Lyrae stars are shown by blue and red filled circles respectively. Selected outliers from Kepley et al. are shown by green triangles and subdwarf outliers from Smith et al. (2009) by yellow open circles.

Table 2. Numbers of stars that are *outliers* and in the *Main Concentration* in the Anticentre and North Galactic Pole Fields.

Field [†]	No. in Main Conc.	No. of Outliers	Per cent. of Outliers	$\langle R_{gal} \rangle$ <i>M.C.</i> (kpc)	$\langle R_{gal} \rangle$ <i>outliers</i> (kpc)
ANTICENTRE BHB	15	14	48%	12.5 ± 0.4	14.1 ± 0.4
ANTICENTRE RR	9	6	40%	11.2 ± 0.6	12.5 ± 0.7
ANTICENTRE BHB + RR	24	20	45%	12.0 ± 0.4	13.6 ± 0.5
NGP BHB	51	9	15%	9.7 ± 0.2	11.4 ± 0.4
NGP RR	22	9	29%	10.2 ± 0.3	11.2 ± 0.6
NGP BHB + RR	73	18	20%	9.8 ± 0.2	11.3 ± 0.3

Notes to Table:

[†] The Anticentre fields are those described in this paper and the Fields at the NGP are those described in Kinman et al. (2007b).

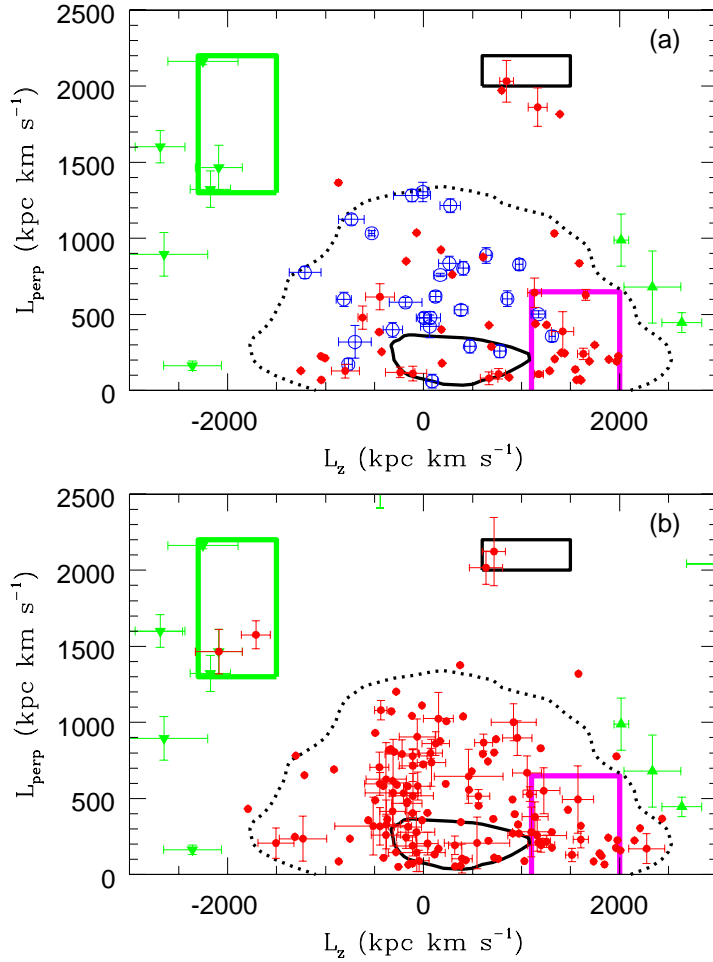


Figure 5. A plot of L_{\perp} against L_z for (a) stars within 1 kpc and (b) those with distances from between one and two kpc. The red filled circles are RR Lyrae stars taken from the catalogue of Maintz & de Boer (2005). Local BHB stars are shown by blue open circles and the outliers from Kepley et al. (2007) are shown by green filled triangles. The black contours and black, green and magenta boxes are described in Fig. 4.

have 4 *outliers* that belong to the H99 group (RZ CEP, XZ CYG, CS ERI and TT LYN); MT TEL is a possible retrograde *outlier* that lies just outside the *main concentration*. The RR Lyrae stars at distances between 1 and 2 kpc have 2 *outliers* that belong to the H99 group (TT CNC and AR SER), 2 that belong to the Kepley retrograde group (AT VIR and RV CAP), and one prograde *outlier* (U CAE) besides a number that are on the edge of the *main concentration*. Kepley et al. (2007) found that XZ CYG belongs to the H99 group and CS ERI is also likely to be a member of this group. The H99 and K07 *outlier* groups are discussed further in Appendix F.

Of the 188 RR Lyrae stars within 2 kpc for which we have data, 41 are likely to belong to the thick disc. Of the remaining 147 halo stars, there are 5 in Fig. 5a and 10 in Fig. 5b that formally lie outside the *main concentration* and so would formally be considered *outliers*. Five of those in Fig. 5b, however, lie so close to the boundary of the *main concentration* that (with reasonable assumptions as to their error bars) it seems likely that most belong to the *main concentration*. The 10 certain *outliers* comprise $7 \pm 2\%$ of the

total. If we include the 5 that lie close to the *main concentration* boundary, there are 15 *outliers* or $10 \pm 3\%$ of the total. These percentages are comparable with those found (10%) by both Helmi et al. (1999) and Morrison et al. (2009) among their local samples of metal-poor halo stars.

Table 2 gives the number of stars in the *main concentration* and the number of *outliers* for the BHB and RR Lyrae stars within 8.5 kpc in both the Anticenter and NGP (Kinman et al. 2007) fields. The percentage of *outliers* and the L_{\perp} of the stars in these fields is shown plotted against galactocentric distance in Figs. 8(a) and 8(b) respectively. It can be seen from Fig. 4 and Fig 8(b) that the majority of *outliers* have greater L_{\perp} and more negative L_z than the stars in the *main concentration*. This shows, according to the correlations shown in Fig. 7, that the orbits of the *outliers* tend to be more retrograde and reach larger $|z_{max}|$ than the stars in the *main concentration*. The increase in the percentage of *outliers* with galactocentric distance shown in Fig. 8(a) therefore implies that as the galactocentric distance increases, the halo has an increas-

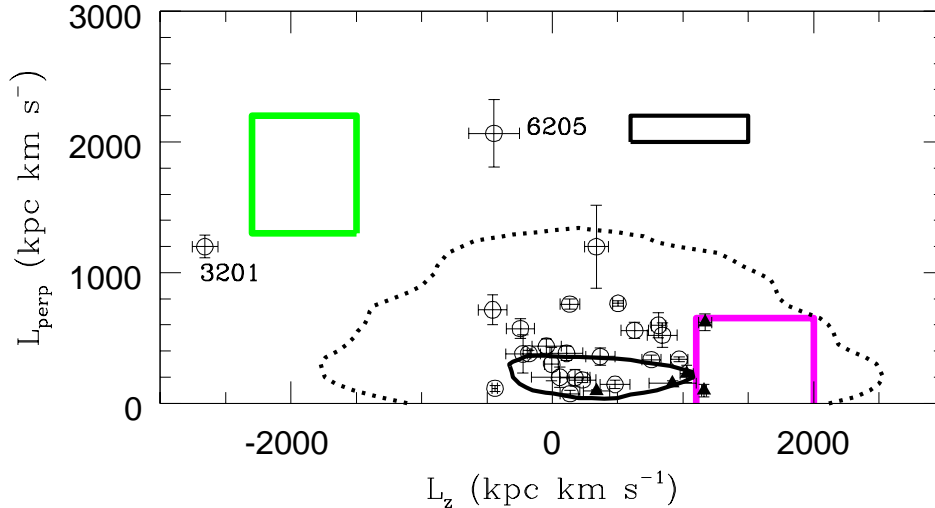


Figure 6. A plot of L_{\perp} against L_z for globular clusters that are within 10 kpc. The two outlying clusters NGC 3201 and NGC 6205 (M13) are indicated by their NGC numbers. Globular clusters with $[\text{Fe}/\text{H}] > -1.0$ are shown by black filled triangles and those with $[\text{Fe}/\text{H}] < -1.0$ by black open circles. The black curves and black, green and magenta boxes are described in Fig. 4.

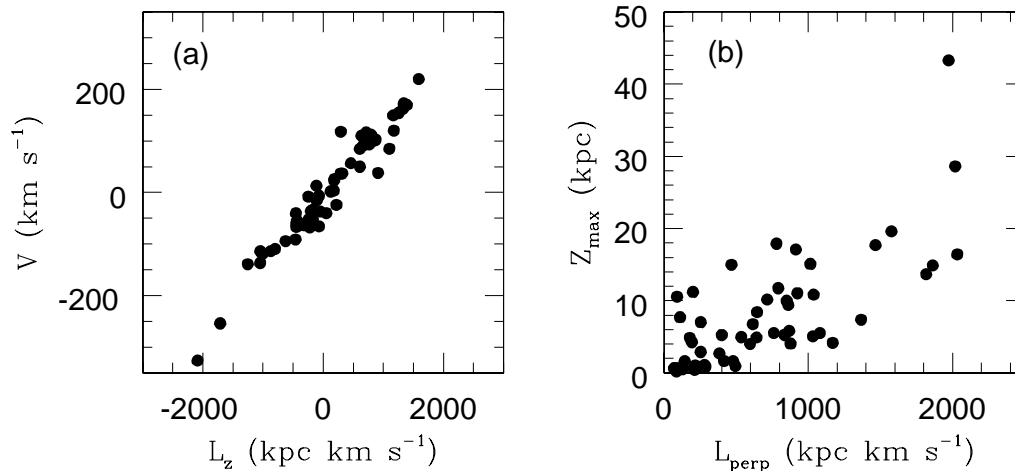


Figure 7. Plots showing the correlation between (a) the galactic rotation V and L_z , and (b) the maximum height of the orbit above the plane (z_{max}) and L_{\perp} . The V and z_{max} are from Maintz & de Boer (2005) for 56 halo RR Lyrae stars.

ing contribution from stars that have more retrograde orbits and a more spherical distribution than the stars in the main concentration that predominate in the solar neighbourhood. This result is in general agreement with the observational results of Carollo et al. (2007,2010) and Beers et al. (2012) and the simulations of Oser et al. (2010), Font et al. (2011) and McCarthy et al. (2012). Our observational support for the duality of the halo is important because (as the simulations have shown) dual halos are a general property of the stellar spheroids of disk galaxies whose masses are comparable with that of the Milky Way. We are grateful to the referee for asking us to emphasize this point.

We note that a simulation of a “smooth halo” with a Gaussian distribution of velocities (e.g. the right-handed L_{\perp} vs. L_z plot of Fig. 5 in Smith et al. 2009) gives a *main concentration* that is similar in shape but smoother than that shown by the observations. In

this connection we note that Hattori & Yoshii (2011) conclude that violent relaxation has been effective for stars within a scale radius of 10 kpc from the Galactic centre. *We suggest that the stars of the main concentration are those where this relaxation has been most effective.*

7 SUMMARY AND CONCLUSIONS

Fifty one BHB stars and 12 possible BHB stars are identified in the Anticentre. Our selection criteria for these stars give results that agree with those used by Smith et al. (2010) and Ruhland et al. (2011). Fifty eight RR Lyrae stars are identified in the Anticentre; 7 of these are new and their light curves are given in Appendix B. Photometric data for the BHB and RR Lyrae stars are given in Ta-

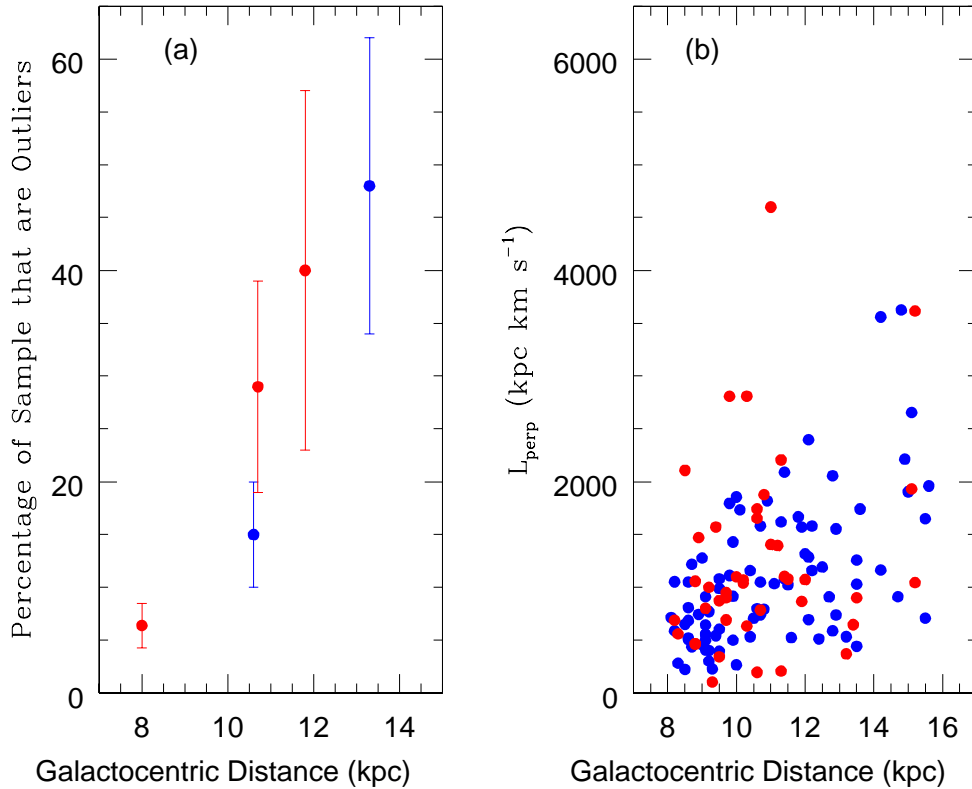


Figure 8. (a) The percentage of outliers in each sample of BHB stars (blue filled circles) and RR Lyrae stars (red filled circles) as a function of Galactocentric distance in kpc. The samples are described in Table 2. (b) The angular momentum L_{\perp} (in kpc km s^{-1}) for the BHB stars (blue filled circles) and RR Lyrae stars (red filled circles) for the NGP and Anticentre samples within 8.5 kpc as a function of Galactocentric distance. *outliers* have a more spherical distribution and more retrograde orbits than those in the *main concentration* and they constitute a larger fraction of the halo with increasing galactocentric distance.

Table 3. Candidates for membership of the K07 group.

Star	Type [†]	L_{\perp} kpc km s^{-1}	L_z kpc km s^{-1}	$\langle V \rangle$ mag.	D kpc	[Fe/H]	Period days
HD 214925	RG ^a	1322 ± 119	-2177 ± 205	9.30	2.15	-2.15	...
AT VIR	RR ^a	1576 ± 93	-1712 ± 149	11.34	1.30	-1.60	0.5257
RV CAP	RR ^a	1464 ± 146	-2090 ± 239	11.04	1.06	-1.72	0.4477
RR7-066	BHB ^b	1960 ± 1028	-1533 ± 645	15.31	8.47
CHSS 608	BHB ^b	1742 ± 452	-2152 ± 657	14.81	6.76
AF-115	BHB ^c	1571 ± 457	-1484 ± 494	15.42	8.13
SA57-032	BHB ^c	1621 ± 604	-1514 ± 670	15.13	7.81
AF-041	BHB ^c	1668 ± 511	-1928 ± 635	15.02	7.46
AF-053	BHB ^c	2091 ± 768	-1609 ± 828	15.19	6.94
SA57-001	BHB ^c	1430 ± 342	-1742 ± 503	14.43	5.68
AF-108	BHB ^c	1279 ± 224	-2185 ± 370	13.86	3.82
IP COM	RR ^c	1878 ± 780	-1860 ± 780	14.85	7.25	-1.48	0.6406
EO COM	RR ^c	1743 ± 483	-1889 ± 528	14.74	6.94	-1.67	0.6320
MQ COM	RR ^c	1572 ± 393	-1895 ± 501	14.23	5.40	...	0.6224
IS COM	RR ^c	1472 ± 177	-1642 ± 338	13.80	4.44	...	0.3146

Notes to Table:

[†] RG = red giant; BHB = blue horizontal branch star; RR = RR Lyrae star. The superscripts a, b & c indicate that the star belongs to the solar neighbourhood, the Anticentre fields of the present paper or the NGP fields of Kinman et al. (2007b) respectively.

bles 4 and 5 respectively. Five methods are used to get distances for the BHB stars and three methods for the RR Lyrae stars; these are compared and combined to give distances on a uniform scale. Absolute proper motions (largely derived from the GSCII and SDSS DR7 databases) are given for all these stars and also radial velocities for 31 of the BHB and 37 of the RR Lyrae stars (Tables 6 and 7). Our conclusions are itemized below:

(i) All but 4 of the 58 RR Lyrae stars in the Anticentre fields are of Oosterhoff type I; this agrees with the Oo II stars being more centrally concentrated in the Galaxy than those of Oo type I (Miceli et al. 2008). Oo I globular clusters tend to have retrograde orbits (Lee & Carney, 1999; van den Bergh, 1993); the field RR Lyrae stars in the Anticentre tend to have retrograde orbits.

(ii) We combined the kinematic data of our Anticentre stars with those of the stars in the North Galactic Pole fields (Kinman et al. 2007b). In the combined data, the Galactic V motion (Fig. 3) is significantly retrograde for *both* BHB and RR Lyrae stars with $R_{gal} > 10$ kpc. This agrees with the findings of Carollo et al. (2007), Carollo et al. (2010) and Beers et al. (2012) that the *outer halo* shows retrograde rotation compared with the rotation of the stars in the solar neighbourhood where the *inner halo* predominates. The lack of any similar trend in the Galactic U motion makes it unlikely that the trend in the V motion is caused by a systematic error in the proper motions.

(iii) Angular momenta plots (L_{\perp} vs. L_z) for the BHB and RR Lyrae stars in the Anticentre fields and the North Galactic Pole fields are compared with similar plots for these stars in the solar neighbourhood and for the globular clusters nearer than 10 kpc. We suggest that halo stars belong to either of two groups — either the *main concentration* or the *outliers* — according to whether they lie inside or outside a contour in this plot which encloses the majority of metal-poor stars in the solar neighbourhood (as defined by Morrison et al. 2009). We suggest that the stars in the *main concentration* are those for which violent relaxation has been most effective (Hattori & Yoshii, 2011). The ratio of *outliers* to *main concentration* stars increases with galactocentric distance (Fig. 8). The *outliers* primarily have retrograde orbits. Since L_{\perp} correlates with z_{max} (the orbit's maximum height above the galactic plane), this also implies that the halo becomes more spherical with increasing galactocentric distance (c.f. Schmidt, 1956; Kinman et al., 1966, Miceli et al., 2008 Table 2). It also agrees with the simulations (McCarthy et al., 2012) that predict that the inner halo should be more flattened than the outer halo.

(iv) A review of the RR Lyrae stars in the H99 group of *outliers* (Helmi et al. 1999) shows that there are six RR Lyrae stars that are likely members (all probably of Oo type I) and that their mean [Fe/H] is -1.59 . Their mean *rms* scatter in [Fe/H] is 0.16 which is comparable with the likely errors in these metallicities. These RR Lyrae stars therefore form a more homogeneous set than the later-type stars in H99 (Roederer et al. 2010) and they could have originated from a single globular cluster. Another grouping with similar L_{\perp} and L_z (which we call K07) contains 15 BHB and RR Lyrae stars at distances in the range 1.1 to 8.5 kpc. K07 contains two pairs of RR Lyrae stars (AT VIR & RV CAP and IP COM & EO COM); the stars in each pair have similar properties. Better data are needed to verify membership of the other stars in K07.

allowing us to use her program for computing L_{\perp} and L_z and the referee for comments which helped improve the paper. This research has made use of 2MASS data provided by the NASA/IPAC Infrared Science Archive, which is operated by the Jet Propulsion Laboratory, California Institute of Technology, under contract with the National Aeronautics and Space Administration.

The GSCII is a joint project of the Space Telescope Science Institute (STScI) and the INAF-Osservatorio Astronomico di Torino (INAF-OATo).

This work is partly based on observations made with the Italian Telescopio Nazionale Galileo (TNG) operated on the island of La Palma by the Fundacion Galileo Galilei of the INAF (Istituto Nazionale di Astrofisica) at the Spanish Observatorio del Roque de los Muchachos of the Instituto de Astrofisica de Canarias.

This work has been partly supported by the MIUR (Ministero dell'Istruzione, dell'Università e della Ricerca) under PRIN-2001-1028897 and PRIN-2005-1060802.

ACKNOWLEDGMENTS

We thank D.R. Soderblom for kindly making available the program to calculate the UVW space motions and Heather Morrison for al-

Table 4. Positions and Photometry for the BHB candidate stars. The equatorial coordinates are for J2000. The magnitudes and colours $V, B, (u - B)_K, NUV$ and K are defined in the text. W is a weight and its relation to the Type (column 14) is given in Appendix A.

No (1)	ID (2)	RA (3)	DEC (4)	l (5)	b (6)	V (7)	$B - V$ (8)	$(u - B)_K$ (9)	$E(B - V)$ (10)	NUV (11)	K (12)	W (13)	Type (14)	Note (15)
1	BS 17438-0126	08 04 07.0	+38 10 30	182.5	+30.00	13.55±0.01	+0.215±0.006	1.985±0.010	0.046	16.146±0.004	12.800±0.024	-6	A	
2	P 54-32.5	08 05 30.9	+41 08 02	179.2	+30.9	15.38±0.01	+0.137±0.013	2.026±0.013	0.064	17.904±0.033	14.813±0.094	+4	bhb	
3	AF 186	08 06 11.1	+40 15 01	180.3	+30.8	15.66±0.01	+0.155±0.013	2.121±0.013	0.055	18.238±0.014	15.281±0.120	+8	BHB	
4	AF 189	08 09 21.8	+38 18 00	182.6	+31.0	15.20±0.01	+0.085±0.016	2.137±0.043	0.048	17.616±0.029	15.108±0.133	+8	BHB	
5	P 54-111	08 12 06.5	+38 50 53	182.1	+31.7	14.58±0.01	+0.136±0.009	2.119±0.013	0.039	17.232±0.008	14.053±0.053	+8	BHB	
6	P 54-122	08 16 00.3	+40 10 00	180.7	+32.6	15.17±0.01	+0.036±0.008	1.965±0.013	0.045	15.152±0.140	+4	bhb	
7	P 54-120	08 16 02.9	+39 25 11	181.6	+32.5	12.49±0.01	+0.216±0.002	1.984±0.005	0.039	15.400±0.010	11.940±0.022	-3	A	
8	P 54-119	08 17 41.6	+39 04 29	182.1	+32.8	14.26±0.01	+0.214±0.007	2.087±0.011	0.038	17.254±0.023	13.532±0.039	+6	BHB	
9	BS 17444-0025	08 21 33.5	+42 31 36	178.2	+34.0	10.11±0.01	+0.136±0.005	2.138±0.005	0.052	09.684±0.013	+4	bhb	1
10	AF 209	08 21 48.5	+42 27 36	178.2	+34.1	16.41±0.02	+0.056±0.022	2.042±0.032	0.051	18.889±0.031	>15.43	+6	BHB	
11	AF 210	08 21 59.7	+42 18 55	178.4	+34.1	15.42±0.01	+0.189±0.012	0.051	18.090±0.020	15.339±0.189	+4	bhb	
12	AF 214	08 22 51.5	+36 18 04	185.6	+33.3	15.66±0.01	+0.226±0.014	2.088±0.020	0.058	18.751±0.049	15.126±0.126	+8	BHB	
13	RR7 002	08 22 00.6	+37 09 40	184.5	+33.3	15.13±0.01	+0.201±0.010	2.167±0.020	0.058	18.119±0.031	14.412±0.086	+8	BHB	2
14	P 81-42	08 23 47.9	+44 32 44	175.8	+34.7	14.43±0.01	+0.050±0.004	2.039±0.011	0.045	16.622±0.010	14.142±0.059	+8	BHB	
15	RR7 008	08 24 09.6	+41 43 47	179.2	+34.4	15.14±0.01	+0.118±0.010	2.120±0.020	0.043	17.601±0.010	14.510±0.081	+8	BHB	3
16	RR7 015	08 26 30.4	+38 10 16	183.5	+34.3	11.75±0.01	+0.208±0.010	2.081±0.020	0.042	11.007±0.020	+10	BHB	4
17	P 81-39	08 27 16.7	+45 18 10	174.9	+35.3	15.69±0.01	+0.035±0.008	2.002±0.011	0.031	17.902±0.023	15.200±0.176	+8	BHB	
18	RR7 021	08 28 02.3	+40 21 57	181.0	+34.9	15.33±0.01	+0.104±0.010	2.118±0.020	0.042	18.088±0.032	14.885±0.131	+1	bhb	
19	P 81-72	08 28 14.1	+44 40 46	175.7	+35.5	11.79±0.01	+0.202±0.001	2.024±0.003	0.028	11.281±0.019	+1	bhb	5
20	P 81-79	08 28 19.9	+45 26 09	174.8	+35.5	13.37±0.01	+0.243±0.002	1.999±0.005	0.026	16.445±0.004	12.732±0.025	-6	A	
21	RR7 023	08 28 29.6	+40 27 47	180.9	+35.0	12.64±0.01	+0.059±0.010	2.111±0.020	0.044	14.926±0.007	12.347±0.022	+9	BHB	6
22	RR7 036	08 32 26.5	+39 27 25	182.2	+35.7	15.25±0.01	+0.165±0.010	2.137±0.020	0.044	18.000±0.046	14.765±0.102	+12	BHB	7
23	P 81-101	08 34 24.5	+46 00 23	174.2	+36.6	15.43±0.01	+0.154±0.015	2.116±0.020	0.029	18.146±0.029	14.620±0.070	+5	bhb	
24	P 81-121	08 35 25.7	+44 00 41	176.7	+36.7	15.65±0.01	+0.045±0.012	1.975±0.014	0.030	17.676±0.011	15.316±0.149	+8	BHB	
25	RR7 043	08 35 29.7	+42 01 19	179.1	+36.5	16.62±0.01	+0.036±0.015	1.986±0.020	0.027	18.721±0.034	15.853±0.238	+8	BHB	8
26	P 28-045	08 37 42.5	+36 07 28	186.5	+36.2	14.315±0.01	+0.135±0.008	2.133±0.021	0.035	13.809±0.042	+4	bhb	
27	RR7 053	08 38 52.8	+40 54 32	180.6	+37.0	15.05±0.01	+0.160±0.010	2.175±0.020	0.041	17.782±0.033	14.4:	+8	BHB	9
28	P 81-162	08 39 57.3	+46 26 45	173.7	+37.6	16.05±0.01	+0.071±0.021	2.047±0.015	0.027	18.341±0.010	15.819±0.228	+8	BHB	10
29	RR7 058	08 40 47.5	+38 13 49	184.0	+37.1	15.43±0.01	+0.064±0.010	2.020±0.020	0.041	17.641±0.026	15.055±0.124	+8	BHB	11
30	RR7 060	08 42 16.8	+36 45 35	185.9	+37.2	14.49±0.01	+0.160±0.010	2.102±0.020	0.035	17.164±0.023	13.836±0.055	+11	BHB	12
31	P 82-04	08 42 41.3	+42 47 07	178.3	+37.9	15.84±0.02	+0.061±0.014	2.069±0.029	0.033	18.123±0.027	15.544±0.208	+8	BHB	13
32	RR7 064	08 43 04.9	+41 39 05	179.7	+37.9	11.22±0.01	+0.115±0.010	2.100±0.010	0.032	10.820±0.018	+8	BHB	14
33	RR7 066	08 43 40.9	+39 49 20	182.1	+37.8	15.31±0.01	+0.130±0.010	2.087±0.020	0.035	17.901±0.030	14.771±0.108	+8	BHB	15
34	P 81-167	08 45 20.2	+46 41 34	173.4	+38.5	14.44±0.01	+0.109±0.008	2.119±0.014	0.035	16.957±0.027	13.959±0.049	+8	BHB	
35	P 11419-01	08 46 48.8	+29 49 04	194.6	+36.8	12.79±0.01	+0.123±0.006	2.079±0.024	0.043	15.376±0.010	12.348±0.022	+9	BHB	16
36	RR7 082	08 47 09.9	+42 16 04	179.0	+38.7	10.69±0.01	+0.069±0.002	1.972±0.003	0.028	10.475±0.018	-3	A	17
37	AF 293	08 47 41.0	+36 10 50	186.8	+38.2	16.24±0.01	+0.193±0.013	2.055±0.036	0.031	18.904±0.015	15.435±0.189	+8	BHB	
38	P 11419-04	08 47 59.8	+31 31 06	192.6	+37.4	14.88±0.01	+0.044±0.004	2.017±0.017	0.038	17.028±0.022	14.739±0.087	+8	BHB	
39	RR7 084	08 48 15.0	+40 28 45	181.3	+38.8	15.76±0.01	+0.141±0.010	2.097±0.020	0.028	18.476±0.024	15.148±0.143	+8	BHB	18
40	RR7 091	08 49 10.7	+39 40 06	182.4	+38.9	14.16±0.01	+0.042±0.010	2.046±0.020	0.026	16.343±0.010	13.906±0.043	+12	BHB	19

Table 4. Continued.

No (1)	ID (2)	RA (3)	DEC (4)	l (5)	b (6)	V (7)	B - V (8)	(u - B) _K (9)	E(B - V) (10)	NUV (11)	K (12)	W (13)	Type (14)	Note (15)
41	RR7 090	08 49 23.3	+40 23 40	181.5	+39.0	15.65±0.01	+0.089±0.010	2.090±0.020	0.024	18.028±0.019	15.285±0.125	+8	BHB	20
42	P 82-49	08 53 25.8	+44 26 21	176.3	+39.9	15.48±0.01	+0.108±0.008	2.099±0.017	0.029	17.905±0.032	14.977±0.103	+8	BHB	21
43	BS 16473-0090	08 57 34.5	+43 28 21	177.6	+40.7	10.91±0.01	+0.215±0.010	1.991±0.010	0.023	10.414±0.020	0	A	
44	BS 16473-0102	08 58 27.1	+47 04 08	172.8	+40.8	13.93±0.01	+0.103±0.005	2.092±0.017	0.021	16.338±0.014	13.504±0.033	+8	BHB	
45	BS 17139-0069	09 06 14.4	+30 58 33	194.3	+41.2	14.45±0.01	+0.146±0.004	2.073±0.015	0.025	17.052±0.044	13.879±0.046	+8	BHB	
46	TON 384	09 06 56.8	+30 04 20	195.5	+41.1	15.25±0.01	+0.056±0.011	2.126±0.061	0.028	17.721±0.035	14.759±0.078	+4	bhb	22
47	BS 16468-0026	09 07 13.9	+40 23 48	181.7	+42.4	14.72±0.01	+0.077±0.005	2.089±0.054	0.020	17.101±0.018	14.186±0.045	+8	BHB	
48	AF 379	09 10 37.1	+38 55 10	183.8	+43.0	15.26±0.02	+0.064±0.010	2.018±0.023	0.019	17.547±0.026	15.149±0.139	+8	BHB	
49	AF 386	09 13 30.0	+36 49 22	186.7	+43.4	15.01±0.01	+0.088±0.005	2.005±0.032	0.020	17.476±0.370	14.679±0.089	+6	BHB	
50	AF 390	09 15 35.7	+38 36 12	184.3	+43.9	15.37±0.01	+0.042±0.025	2.091±0.020	0.019	17.497±0.022	15.117±0.149	+8	BHB	
51	BS 16468-0078	09 16 19.4	+40 16 02	181.9	+44.1	11.67±0.01	+0.024±0.001	1.998±0.010	0.014	11.446±0.017	+7	BHB	23
52	P 30-16	09 16 53.1	+35 52 17	188.1	+44.0	14.40±0.01	+0.123±0.006	2.058±0.030	0.019	13.879±0.055	+4	bhb	
53	BS 16468-0080	09 17 13.4	+41 20 43	180.5	+44.2	14.09±0.01	+0.023±0.009	1.900±0.017	0.021	15.915±0.012	14.009±0.057	+4	bhb	
54	P 30-28	09 17 44.4	+33 20 52	191.6	+43.9	10.28±0.01	+0.119±0.004	2.083±0.003	0.018	09.757±0.016	+7	BHB	24
55	BS 16468-0090	09 18 25.8	+39 29 59	183.0	+44.5	14.10±0.01	+0.132±0.011	2.075±0.004	0.016	16.674±0.017	13.676±0.045	+8	BHB	
56	CHSS 608	09 18 59.0	+29 40 46	196.7	+43.6	14.81±0.01	+0.089±0.011	2.045±0.030	0.021	17.276±0.023	14.353±0.071	+11	BHB	
57	P 11424-28	09 20 23.3	+31 17 11	194.5	+44.2	14.50±0.01	+0.104±0.007	2.049±0.024	0.023	17.052±0.022	14.008±0.053	+8	BHB	
58	P 30-38	09 21 27.6	+35 24 14	188.8	+44.9	14.39±0.01	+0.142±0.015	2.046±0.050	0.018	17.029±0.016	13.929±0.057	+8	BHB	
59	57-121	09 25 48.5	+39 04 30	183.7	+45.9	15.25±0.02	+0.005±0.020	2.040±0.033	0.014	17.310±0.025	15.396±0.209	+6	BHB	
60	AF 419	09 25 56.3	+28 50 07	198.2	+45.0	15.19±0.02	+0.113±0.016	2.100±0.043	0.019	17.636±0.029	14.611±0.093	+9	BHB	25
61	P 11424-70	09 30 02.7	+31 54 14	194.1	+46.3	14.57±0.01	+0.072±0.019	2.072±0.032	0.020	16.939±0.019	14.236±0.073	+8	BHB	
62	BS 16927-22	09 32 43.6	+39 28 31	183.1	+47.3	11.18±0.01	+0.103±0.005	2.084±0.011	0.017	10.710±0.019	+4	bhb	
63	CHSS 663	09 33 48.8	+29 07 14	198.2	+46.7	15.18±0.01	+0.056±0.011	2.077±0.035	0.018	17.282±0.024	14.959±0.112	+12	BHB	
64	P 11424-82	09 34 23.5	+29 48 10	197.3	+46.9	14.99±0.01	+0.136±0.017	2.115±0.048	0.019	17.554±0.026	14.379±0.068	+8	BHB	
65	BS 16940-45	09 37 07.2	+36 09 48	188.0	+48.1	13.55±0.01	+0.021±0.011	2.009±0.008	0.014	15.602±0.015	13.336±0.030	+8	BHB	
66	BS 16927-55	09 40 31.5	+41 48 32	179.5	+48.6	14.53±0.01	+0.003±0.005	1.993±0.046	0.012	16.592±0.023	14.276±0.064	+6	BHB	
67	BS 16940-0070	09 42 36.7	+34 38 18	190.4	+49.1	14.98±0.01	+0.016±0.008	2.002±0.083	0.011	17.201±0.031	14.815±0.077	+4	bhb	
68	BS 16940-0072	09 43 10.3	+33 57 10	191.4	+49.2	13.99±0.01	+0.107±0.008	2.032±0.004	0.014	16.453±0.015	13.524±0.027	+8	BHB	

Notes to table:

- (1) BD +42 1850; (2) AF 211; (3) AF 217; (4) Strömgren $\beta = 2.758$; CHSS (class 3); (5) Strömgren $\beta = 2.855$;
(6) Strömgren $\beta = 2.879$; CHSS (class 3); (7) CHSS (class 4); (8) AF 241; (9) AF 256; (10) US 1430;
(11) AF 262. (12) CHSS (class 3); (13) US 1513; (14) Strömgren $\beta = 2.856$; CHSS (class 3); (15) AF 271;
(16) Strömgren $\beta = 2.801$; (17) Strömgren $\beta = 2.892$; (18) AF 297; (19) CHSS (class 4); (20) AF 307;
(21) BD +42 1926; US 1862; (22) AF 368; (23) Strömgren $\beta = 2.858$;
(24) Strömgren $\beta = 2.827$; BD +33 1834; (25) CHSS 632 (class 1).

References to Notes:

AF nnn (Pesch & Sanduleak, 1989); CHSS (Brown et al., 2003);
US nnnn (Usher & Mitchell, 1982).

Table 5. Positions, Photometry and Abundances for the RR Lyrae stars. The equatorial coordinates are for J2000. The magnitudes and colours V and K are defined in the text. Sources are given in the Notes.

No (1)	ID (2)	RA (3)	DEC (4)	l (5)	b (6)	Type (7)	logP (8)	[Fe/H] (9)	$\langle V \rangle$ (10)	V_{amp} (11)	$\langle K \rangle$ (12)	$E(B - V)$ (13)	Notes (14)
1	V385 Aur	07 25 56.0	+38 12 59	180.3	+22.8	<i>ab</i>	-0.266	...	(17.41)	(0.59)	...	0.053	
2	V386 Aur	07 26 13.2	+40 52 50	177.6	+23.6	<i>c</i>	-0.516	-1.75	(16.75)	(0.50)	...	0.063	5
3	V387 Aur	07 27 01.0	+36 38 46	182.0	+22.5	<i>ab</i>	-0.308	-1.32	(16.92)	(1.05)	...	0.056	5
4	V389 Aur	07 30 10.8	+38 21 54	180.4	+23.6	<i>ab</i>	-0.249	...	(17.53)	(0.95)	...	0.057	
5	VX Lyn	07 31 51.9	+39 07 47	179.7	+24.1	<i>ab</i>	-0.257	-1.58	17.01	(0.82)	...	0.057	4
6	VY Lyn	07 32 26.0	+38 50.05	180.1	+24.2	<i>c</i>	-0.451	-1.57	15.75	(0.37)	14.61±0.12	0.062	4
7	VZ Lyn	07 32 40.8	+41 37 38	177.1	+25.0	<i>c</i>	-0.487	-1.48	16.20	(0.42)	15.43±0.19	0.054	4
8	WX Lyn	07 35 38.5	+39 15 27	179.8	+24.9	<i>ab</i>	-0.257	-1.72	16.84	(0.69)	...	0.049	4
9	AS Lyn	07 40 32.9	+41 11 37	178.0	+26.3	<i>ab</i>	-0.298	-1.2:	(18.35)	1.05	...	0.049	1
10	WZ Lyn	07 40 45.7	+39 18 51	180.1	+25.8	<i>ab</i>	-0.207	-1.89	(14.25)	(0.95)	13.11±0.03	0.049	2
11	XZ Lyn	07 44 48.4	+40 12 44	179.3	+26.8	<i>c</i>	-0.549	...	(16.32)	(0.50)	...	0.050	
12	TW Lyn	07 45 06.3	+43 06 42	176.1	+27.5	<i>ab</i>	-0.317	-0.43	11.99	1.00	10.78±0.02	0.046	3,8
13	YY Lyn	07 45 30.1	+37 22 59	182.4	+26.2	<i>c</i>	-0.476	-1.87	14.98	(0.46)	14.08±0.11	0.065	4
14	YZ Lyn	07 45 40.9	+40 22 32	179.2	+27.0	<i>ab</i>	-0.304	-0.6:	(17.47)	(0.80)	...	0.052	1
15	AU Lyn	07 49 35.3	+41 42 57	177.9	+28.0	<i>ab</i>	-0.197	-1.8:	(17.82)	(0.76)	...	0.048	1
16	ZZ Lyn	07 50 21.8	+37 42 00	182.3	+27.3	<i>ab</i>	-0.313	-1.42	15.80	(1.03)	15.08±0.14	0.048	4
17	RW Lyn	07 50 39.2	+38 27 15	181.5	+27.5	<i>ab</i>	-0.302	-1.53	12.90	(1.20)	11.66±0.02	0.040	4,9
18	AV Lyn	07 54 09.6	+42 49 04	176.9	+29.1	<i>ab</i>	-0.233	-1.7:	(16.62)	(0.76)	...	0.048	1
19	AC Lyn	07 54 42.1	+38 54 20	181.2	+28.4	<i>ab</i>	-0.256	-1.50	16.38	(0.85)	...	0.047	4
20	AD Lyn	07 56 23.0	+39 22 58	180.8	+28.8	<i>c</i>	-0.450	-1.46	15.85	(0.49)	15.13±0.15	0.061	4
21	AW Lyn	07 57 24.5	+43 12 29	176.5	+29.8	<i>ab</i>	-0.333	-1.6:	(16.13)	(0.92)	15.00±0.11	0.036	1
22	AX Lyn	07 59 46.4	+39 16 30	181.1	+29.4	<i>ab</i>	-0.331	...	(18.54)	(0.76)	...	0.048	
23	AY Lyn	08 00 29.9	+40 39 24	179.6	+29.8	<i>c</i>	-0.503	...	(16.88)	(0.47)	...	0.045	
24	P 54-13	08 01 56.2	+41 01 18	179.2	+30.2	<i>ab</i>	-0.226	...	15.20	0.90	13.52±0.04	0.058	6
25	AZ Lyn	08 03 39.8	+42 30 45	177.6	+30.7	<i>ab</i>	-0.324	-2.24	16.47	(0.84)	...	0.046	5
26	BB Lyn	08 04 36.2	+42 29 01	177.6	+30.9	<i>ab</i>	-0.253	-1.36	(16.86)	(0.92)	...	0.048	5
27	BC Lyn	08 09 37.4	+42 33 31	177.7	+31.9	<i>ab</i>	-0.281	-1.6:	(17.00)	(1.07)	...	0.048	1
28	AF 194	08 12 00.6	+40 39 20	180.0	+32.0	<i>ab</i>	-0.075	...	15.84	0.45	14.37±0.08	0.048	7
29	AF 197	08 13 46.4	+38 03 02	183.1	+31.8	<i>c</i>	-0.411	...	15.50	0.40	14.35±0.07	0.038	7
30	DQ Lyn	08 23 41.0	+37 28 11	184.2	+33.6	<i>c</i>	-0.306	...	11.41	0.37	10.44±0.02	0.044	6
31	RR7 032	08 30 41.8	+40 24 24	181.0	+35.4	<i>ab</i>	-0.201	...	14.58	0.65	13.22±0.03	0.047	6
32	RR7 034	08 31 52.2	+38 32 14	183.3	+35.4	<i>c</i>	-0.539	...	15.32	0.29	14.64±0.09	0.039	6
33	P 81 129	08 32 49.6	+43 16 02	177.5	+36.2	<i>c</i>	-0.510	...	14.46	0.52	13.67±0.04	0.022	6
34	AF Lyn	08 35 57.4	+41 01 11	180.4	+36.5	<i>ab</i>	-0.237	-1.56	16.12	(0.76)	14.87±0.09	0.039	4
35	P 82 06	08 43 56.7	+43 22 13	177.6	+38.2	<i>c</i>	-0.548	...	14.15	0.30	13.45±0.03	0.024	6
36	AI Lyn	08 44 02.6	+38 54 48	183.2	+37.8	<i>ab</i>	-0.250	...	(17.10)	(0.92)	...	0.032	
37	AK Lyn	08 45 55.1	+39 14 55	182.8	+38.2	<i>ab</i>	-0.329	-1.56	16.00	(1.07)	14.86±0.11	0.030	4
38	EN Lyn	08 46 07.0	+38 02 53	184.4	+38.1	<i>ab</i>	-0.204	...	13.53	0.52	12.18±0.02	0.035	6
39	RR7-086	08 48 26.2	+36 20 08	186.6	+38.4	<i>c</i>	-0.451	...	16.14	0.63	15.51±0.15	0.029	7
40	AL Lyn	08 49 13.1	+38 49 31	183.5	+38.8	<i>ab</i>	-0.293	-1.90	16.52	(0.99)	15.18±0.11	0.035	4
41	AM Lyn	08 49 50.2	+36 56 00	185.9	+38.7	<i>ab</i>	-0.294	...	(17.30)	(1.31)	...	0.033	
42	P 82-32	08 50 39.5	+43 40 03	177.3	+39.4	<i>ab</i>	-0.304	...	15.07	1.16	14.24±0.06	0.031	6
43	AF 316	08 50.46.3	+41 18 54	180.3	+39.3	<i>c</i>	-0.462	...	16.13	0.46	15.09±0.12	0.027	7
44	RR7-101	08 51 40.2	+40 17 11	181.6	+39.4	<i>c</i>	-0.482	...	16.15	0.60	15.14±0.11	0.022	7
45	TT Lyn	09 03 07.8	+44 35 08	176.1	+41.7	<i>ab</i>	-0.224	-1.35	09.85	0.70	08.61±0.02	0.018	10,11
46	AF 400	09 18 17.0	+31 58 49	193.5	+43.9	<i>c</i>	-0.403	...	14.10	0.40	13.37±0.03	0.018	7
47	AF 430	09 30 23.3	+33 53 11	191.2	+46.6	<i>c</i>	-0.515	...	14.90	0.40	14.21±0.04	0.016	7
48	BS 16927-123	09 44 36.4	+41 08 39	180.4	+49.4	<i>c</i>	-0.445	...	13.18	0.46	12.36±0.02	0.017	6
49	X LMi	10 06 06.7	+39 21 28	182.5	+53.7	<i>ab</i>	-0.165	-1.41	12.35	1.02	11.06±0.01	0.018	12,13
50	AG UMa	10 48 56.3	+42 40 14	172.9	+60.7	<i>ab</i>	-0.335	...	(15.42)	1.71	14.53±0.10	0.012	14

Table 5. Continued.

No	ID	RA	DEC	l	b	Type	logP	[Fe/H]	$\langle V \rangle$	V_{amp}	$\langle K \rangle$	E(B - V)	Notes
(1)	(2)	(3)	(4)	(5)	(6)	(7)	(8)	(9)	(10)	(11)	(12)	(13)	(14)
51	BK UMa	10 50 18.9	+42 34 08	172.9	+61.0	<i>ab</i>	-0.197	-1.29	12.91	0.54	11.50±0.02	0.012	12,15
52	AK UMa	10 53 13.2	+41 19 02	174.9	+61.9	<i>c</i>	-0.309	...	(16.08)	(0.46)	15.00±0.12	0.012	16
53	AO UMa	11 07 39.8	+40 33 58	174.1	+64.7	<i>ab</i>	-0.251	...	(15.54)	(1.22)	14.62±0.10	0.015	
54	BN UMa	11 16 22.9	+41 14 02	170.9	+65.9	<i>d</i>	-0.398	...	13.50	0.50	12.58±0.03	0.014	6,17
55	CK UMa	12 01 36.4	+31 54 12	186.2	+78.2	<i>ab</i>	-0.214	...	14.08	0.53	12.72±0.03	0.024	6

Notes to table:

(1) [Fe/H] from Saha & Oke (1984). (2) [Fe/H] from private communication from Suntzeff (1990). (3) [Fe/H] from Jurcsik et al. (2006). (4) [Fe/H] and $\langle V \rangle$ from Pier, Saha & Kinman (2003). (5) [Fe/H] and $\langle V \rangle$ from Kinman, Saha & Pier (2004). (6) $\langle V \rangle$ from Kinman & Brown (2010). (7) $\langle V \rangle$ from this paper (appendix). (8) $\langle V \rangle$ from Schmidt, Chab & Reiswig (1995). (9) $\langle V \rangle$ from Schmidt & Seth (1996). (10) $\langle V \rangle$ from Liu & Janes (1990). (11) [Fe/H] from Sodor, Jurcsik & Szeidl (2009). (12) $\langle V \rangle$ from Schmidt (2002). (13) [Fe/H] from Jurcsik & Kovacs (1996). (14) $\langle V \rangle$ from Kinemuchi et al. (2006). (15) [Fe/H] from Kemper (1982). (16) Bailey type and period uncertain. (17) McClusky (2008) showed that this star is an RRd. The period given is that of the first overtone.

Table 6. Parallaxes, Proper Motions, Radial Velocities, Galactic Distances and Galactic Space Velocities for the BHB stars.

No	ID	Π (mas)	μ_α (mas y ⁻¹)	μ_δ (mas y ⁻¹)	S_μ	RV (km s ⁻¹)	S_{RV}	D (kpc)	Z (kpc)	R_{gal} (kpc)	U (km s ⁻¹)	V (km s ⁻¹)	W (km s ⁻¹)	L_\perp (kpc km s ⁻¹)	L_z (kpc km s ⁻¹)
(1)	(2)	(3)	(4)	(5)	(6)	(7)	(8)	(9)	(10)	(11)	(12)	(13)	(14)	(15)	(16)
2	P 54-32.5	0.119±0.002	-1.3±0.6	-0.2±1.6	1	-017.4±4	1	8.4	4.3	15.8	+002±015	+007±061	-047±024	+1299±264	+3445±929
3	AF 186	0.104±0.002	0.0±3.0	-10.0±3.0	3	9.6	4.9	17.0
4	AF 189	0.135±0.004	+4.0±3.0	-5.0±3.0	3	7.4	3.8	14.8
5	P 54-111	0.165±0.003	+4.1±1.4	-19.6±2.4	1	-054.5±4	1	6.1	3.2	13.5	-081±022	-570±067	-016±036	+1258±255	-4615±884
6	P 54-122	0.144±0.004	+3.9±0.5	-7.1±0.8	1	-128.7±4	1	6.9	3.7	14.3	-168±009	-244±027	+011±014	+0808±225	-0348±374
8	P 54-119	0.185±0.003	+1.7±1.2	-20.5±0.9	1	-194.2±4	1	5.4	2.9	12.9	-166±017	-513±025	-139±026	+1554±297	-3697±320
9	BS 17444-0025	1.348±0.031	+5.9±0.6	-27.0±0.6	2	0.7	0.4	8.6
10	AF 209	0.075±0.002	+2.5±3.0	-4.0±3.0	3	13.3	7.5	20.5
11	AF 210	0.111±0.002	+9.0±3.8	0.8±1.3	1	-084.9±4	1	9.0	5.0	16.3	-295±091	-015±060	+277±135	+5938±2401	+3204±925
12	AF 214	0.100±0.002	-1.0±2.0	-1.0±2.0	3	10.0	5.5	17.2
13	RR7 002	0.128±0.002	-5.6±2.2	-8.9±1.7	1	+249.0±4	1	7.8	4.3	15.1	+322±047	-308±066	-081±069	+2655±1139	-1091±957
14	P 81-42	0.191±0.003	-3.0±3.0	-10.0±3.0	3	5.2	3.0	12.7
15	RR7 008	0.129±0.002	-1.2±0.7	-13.6±1.0	1	-005.8±4	1	7.8	4.4	15.0	+054±016	-487±038	-085±023	+1905±329	-3838±548
16	RR7 015	0.592±0.009	-20.2±1.0	-35.0±0.7	2	+238.4±4	1	1.7	1.0	9.4	+287±006	-263±006	-028±007	+0544±075	-0380±066
17	P 81-39	0.106±0.002	-2.0±3.0	-2.0±3.0	3	9.4	5.5	16.6
18	RR7 021	0.120±0.002	-1.9±0.9	-8.3±1.2	1	+092.9±4	1	8.3	4.8	15.6	+129±019	-310±046	-037±027	+1287±454	-1318±686
19	P 81-72	0.575±0.016	-2.5±0.9	-2.8±0.6	2	1.7	1.0	9.5
21	RR7 023	0.436±0.007	+7.7±1.6	-22.6±0.7	2	-059.3±4	1	2.3	1.3	10.0	-091±010	-248±009	+014±014	+0267±140	-0281±087
22	RR7 036	0.121±0.002	-1.5±3.0	-7.5±3.0	3	+160.0±40	3	8.3	4.8	15.5	+171±074	-284±120	+017±099	+1650±1048	-894±1765
23	P 81-101	0.107±0.002	+1.0±3.0	-2.0±3.0	3	9.3	5.6	16.5
24	P 81-121	0.100±0.006	0.0±3.0	-8.0±3.0	3	10.0	6.0	17.1
25	RR7 043	0.067±0.002	+1.0±3.0	-3.0±3.0	3	14.9	8.9	21.9
26	P 28-045	0.186±0.003	-5.0±1.6	-12.2±0.8	1	-356.6±4	1	5.4	3.2	12.7	-225±025	-257±021	-345±034	+3528±498	-0568±265
27	RR7 053	0.132±0.002	-2.9±2.0	-16.0±2.5	1	-241.0±5	2	7.6	4.6	14.8	-111±43	-555±090	-266±057	+3626±916	-4700±1258
28	P 81-162	0.086±0.001	+1.0±3.0	-1.0±3.0	3	11.6	7.1	18.6
29	RR7 058	0.120±0.002	+1.0±0.9	-7.1±1.5	1	+030.0±5	2	8.3	5.0	15.5	-006±023	-279±060	+027±029	+0709±374	-0866±871
30	RR7 060	0.169±0.003	+0.3±1.5	-6.1±1.1	1	+063.2±4	1	5.9	3.6	13.2	+033±025	-168±031	+033±032	+0534±314	+0668±391
31	P 82-04	0.097±0.001	+2.0±3.0	-3.0±3.0	3	10.3	6.3	17.3
32	RR7 064	0.784±0.016	-5.1±0.7	-5.4±0.7	2	+034.8±4	1	1.3	0.8	9.0	+038±004	-024±004	+002±004	+0159±007	+1758±038
33	RR7 066	0.118±0.002	-1.9±2.1	-8.5±1.1	1	-055.0±5	2	8.5	5.2	15.6	+003±054	-325±044	-114±069	+1960±1028	-1533±645
34	P 81-167	0.178±0.003	-10.0±3.0	-2.0±3.0	3	5.6	3.5	12.9
35	P 11419-01	0.386±0.007	+6.1±2.2	-18.3±0.9	1	+287.1±4	1	2.6	1.6	10.1	+141±017	-277±012	+196±021	+1734±238	-0494±124
37	AF 293	0.074±0.001	-5.0±3.0	-6.0±3.0	3	13.5	8.4	20.4
38	P 11419-04	0.157±0.003	-0.8±1.2	-7.1±0.3	1	+170.7±4	1	6.4	3.9	13.5	+116±023	-233±010	+059±028	+0444±319	-0040±139
39	RR7 084	0.094±0.001	0.0±3.0	-7.0±3.0	3	-065.0±40	3	10.6	6.7	17.6	-057±099	-344±151	-050±120	+2533±1425	-2029±2446
40	RR7 091	0.211±0.003	-0.7±1.4	-15.3±.9	1	-041.0±4	1	4.7	3.0	12.1	-027±020	-335±020	-054±024	+0696±256	-1349±235

Table 6. Continued.

No	ID	Π (mas)	μ_α (mas y ⁻¹)	μ_δ (mas y ⁻¹)	S_μ	RV (km s ⁻¹)	S_{RV}	D (kpc)	Z (kpc)	R_{gal} (kpc)	U (km s ⁻¹)	V (km s ⁻¹)	W (km s ⁻¹)	L_\perp (kpc km s ⁻¹)	L_z (kpc km s ⁻¹)
(1)	(2)	(3)	(4)	(5)	(6)	(7)	(8)	(9)	(10)	(11)	(12)	(13)	(14)	(15)	(16)
41	RR7 090	0.101±0.002	+3.0±3.0	-4.0±3.0	3	-112.0±40	3	9.9	6.2	16.9	-180±095	-185±143	+032±111	+2525±1525	+0502±2242
42	P 82-49	0.111±0.002	-2.0±3.0	-4.0±3.0	3	9.0	5.8	16.0
44	BS 16473-0102	0.220±0.004	+8.0±3.0	-12.0±3.0	3	4.5	3.0	11.8
45	BS 17139-69	0.170±0.003	-3.3±0.7	-9.2±1.0	1	+105.4±4	1	5.9	3.9	12.9	+096±014	-265±027	-027±015	+0740±231	-0446±331
46	TON 384	0.124±0.002	-0.7±1.3	-3.6±1.1	1	-174.7±4	1	8.1	5.3	14.9	-140±035	-094±044	-146±039	+1415±582	+1510±610
47	BS 16468-0026	0.154±0.003	-1.8±1.2	-13.4±1.0	1	+211.2±4	1	6.5	4.4	13.5	+181±024	-412±032	+098±027	+1031±231	-2418±418
48	AF 379	0.123±0.003	+3.5±3.0	-9.5±3.0	3	8.1	5.5	15.0
49	AF 386	0.136±0.002	+2.2±0.9	-8.4±1.2	1	+009.6±4	1	7.4	5.1	14.2	-075±022	-286±042	+053±023	+1164±379	-0925±557
50	AF 390	0.118±0.002	-2.0±3.0	-5.0±3.0	3	8.5	5.9	15.3
51	BS 16468-0078	0.654±0.010	-19.8±0.6	-29.1±0.7	2	1.5	1.1	9.2
52	P 30-16	0.173±0.003	+1.0±3.0	-4.7±3.0	3	5.8	4.0	12.8
53	BS 16468-0080	0.224±0.007	+1.4±1.2	-17.9±1.6	1	-001.7±4	1	4.5	3.1	11.6	-037±017	-372±036	+030±018	+0691±184	-1700±405
54	P 30-28	1.161±0.017	+9.5±0.7	-20.6±0.7	2	0.9	0.6	8.6
55	BS 16468-0090	0.200±0.004	-0.4±1.6	-8.0±1.6	1	+221.6±4	..	5.0	3.5	12.1	+145±027	-193±039	+155±027	+1287±404	+0345±446
56	CHSS 608	0.148±0.002	-3.4±1.2	-12.5±1.6	1	+029.0±4	..	6.8	4.7	13.6	+023±029	-393±051	-104±029	+1742±452	-2152±657
57	P 11424-28	0.169±0.003	+1.3±1.4	-7.9±1.6	1	+011.6±4	1	5.9	4.1	12.8	-061±030	-217±043	+017±030	+0589±363	-0030±527
58	P 30-38	0.175±0.003	+2.0±3.0	-11.0±3.0	3	-179.3±4	1	5.7	4.0	12.7	-204±059	-269±079	-096±059	+0911±568	-0716±946
59	57-121	0.125±0.005	-1.8±1.2	-8.6±1.4	1	+066.1±5	2	8.0	5.7	14.7	+066±032	-329±056	+005±031	+0912±391	-1451±760
60	AF 419	0.121±0.003	+3.3±1.0	-6.2±2.2	1	+072.7±4	1	8.3	5.8	14.9	-098±033	-242±086	+116±030	+2213±539	-0479±1186
61	P 11424-70	0.168±0.003	+3.3±1.2	-13.8±2.9	1	+152.7±4	1	6.0	4.3	12.8	-035±028	-397±080	+148±024	+2057±372	-2154±970
62	BS 16927-22	0.773±0.012	+6.8±0.8	-29.8±0.6	2	+082.2±4	1	1.3	1.0	8.9	+003±004	-177±005	+098±004	+0872±039	+0378±041
63	CHSS 663	0.130±0.003	-9.0±2.0	-11.0±2.0	3	7.7	5.6	14.3
64	P 11424-82	0.132±0.002	-6.6±1.4	-14.7±1.3	1	+030.7±4	1	7.6	5.5	14.2	+087±038	-533±047	-187±035	+3559±605	-3896±620
65	BS 16940-45	0.276±0.004	-3.7±1.8	-16.7±1.5	1	-101.0±4	1	3.6	2.7	10.7	-0063±023	-275±025	-116±021	+1050±278	-0594±258
66	BS 16927-55	0.181±0.006	-2.5±0.9	-12.3±1.8	1	+043.1±4	1	5.5	4.1	12.4	+050±018	-323±047	+015±016	+0513±193	-1204±548
67	BS 16940-0070	0.144±0.002	+2.6±1.2	-3.5±1.3	1	-082.3±4	1	6.9	5.3	13.6	-146±030	-091±043	-001±025	+1080±374	+1473±538
68	BS 16940-0072	0.210±0.003	+5.2±1.2	-11.5±1.0	1	-135.1±4	1	4.8	3.6	11.6	-225±020	-223±024	-029±018	+0525±246	-0175±265

Notes to table:

(1) Sources of proper motions (S_μ): (1) GSCII-SDSS (2) Nomad (3) SDSS (DR 7)

(2) Sources of Radial Velocities (S_{RV}): (1) Bologna (2) Kitt Peak 4-m (3) Kinman et al. (1994)

(3) Distances: (D) Heliocentric distance; (Z) Height above Plane; R_{gal} Galactocentric distance assuming Solar Galactocentric Distance = 8.0 kpc

Table 7. Parallaxes, Proper Motions, Radial Velocities, Galactic Distances and Galactic Space Velocities for the RR Lyrae stars.

No	ID	Π (mas)	μ_α (mas y ⁻¹)	μ_δ (mas y ⁻¹)	S_μ	RV (km s ⁻¹)	S_{RV}	D (kpc)	Z (kpc)	R_{gal} (kpc)	U (km s ⁻¹)	V (km s ⁻¹)	W (km s ⁻¹)	L_\perp (kpc km s ⁻¹)	L_z (kpc km s ⁻¹)
(1)	(2)	(3)	(4)	(5)	(6)	(7)	(8)	(9)	(10)	(11)	(12)	(13)	(14)	(15)	(16)
1	V385 Aur	0.044±0.002	-3.4±3.3	+0.6±3.2	1	22.7	8.8	30.3
2	V386 Aur	0.060±0.003	+2.1±2.1	-5.0±1.7	1	+116.0±30.0	3	16.7	6.7	24.2	+091±071	-412±135	+106±152	+3982±2474	-4534±3191
3	V387 Aur	0.057±0.003	+1.4±1.2	-0.6±0.9	1	-003.0±30.0	3	17.5	6.7	25.1	-050±046	-074±080	+092±087	+3223±1794	+3486±1954
4	V389 Aur	0.042±0.002	-1.2±3.0	3.3±0.8	1	23.8	9.5	31.3
5	VX Lyn	0.053±0.003	-1.8±1.2	-4.1±1.9	1	+001.3±15.0	1	18.9	7.7	26.4	+099±049	-296±168	-228±103	+6730±2927	-1919±4259
6	VY Lyn	0.098±0.003	+2.2±1.0	-1.6±2.1	1	+114.5±15.0	1	10.2	4.2	17.8	+061±026	-095±101	129±050	+2097±931	+2160±1743
7	VZ Lyn	0.078±0.004	-1.9±1.4	-2.2±2.2	1	-182.1±15.0	1	12.8	5.4	20.3	-109±044	-095±129	-200±086	+3604±1684	+2498±2548
8	WX Lyn	0.056±0.003	-2.1±1.1	-3.3±1.0	1	+026.3±15.0	1	17.9	7.5	25.3	+121±042	-214±087	-211±086	+6093±2401	+148±2131
9	AS Lyn	0.030±0.002	+1.1±0.7	-3.1±2.0	1	-179.0±46.0	3	33.3	14.8	40.7	-175±078	-502±309	-026±119	+7604±3882	-10531±11848
10	WZ Lyn	0.180±0.004	+1.3±0.6	-13.0±1.2	1	+197.0±20.0	4	5.6	2.4	13.2	+193±020	-337±031	+043±018	+371±107	-1511±411
11	XZ Lyn	0.072±0.004	+2.1±1.6	-1.5±1.0	1	-032.0±20.0	4	13.9	6.3	21.3	-086±051	-125±073	+087±096	+2885±1689	+1926±1482
12	TW Lyn	0.592±0.011	+0.6±3.8	2.6±2.9	1	-039.0±05.0	5	1.7	0.8	9.5	-050±015	+021±022	-002±027	+307±121	+2294±213
13	YY Lyn	0.133±0.002	+5.7±0.7	-5.9±1.4	1	-093.1±15.0	1	7.5	3.3	15.1	-165±018	-249±049	+092±026	+1932±412	-478±723
14	YZ Lyn	0.047±0.002	-0.5±0.7	-3.7±1.3	1	+033.0±40.0	3	21.3	9.7	28.6	+087±051	-349±133	-098±070	+4038±2027	-3482±3594
15	AU Lyn	0.035±0.002	-0.8±1.7	-0.8±2.1	1	+096.0±45.0	3	28.6	13.4	35.8	+139±120	-056±283	-060±209	+8978±5151	+5307±9477
16	ZZ Lyn	0.089±0.001	-1.4±1.4	-1.4±0.9	1	+147.2±15.0	1	11.2	5.1	18.7	+160±034	-054±048	-006±061	+1636±775	+3045±872
17	RW Lyn	0.358±0.016	+7.3±1.7	-15.7±2.5	1	-149.8±15.0	1	2.8	1.3	10.6	-169±016	-216±034	-023±022	+197±139	+32±354
18	AV Lyn	0.062±0.003	+0.5±0.8	-4.9±1.1	1	-126.0±30.0	3	16.1	7.8	23.4	-081±041	-373±084	-87±056	+2114±1030	-3311±1887
19	AC Lyn	0.071±0.004	+1.1±0.9	-5.9±1.2	1	-025.8±15.0	1	14.1	6.7	21.5	-030±031	-395±085	-024±054	+1733±766	-3581±1761
20	AD Lyn	0.088±0.006	+1.2±1.1	-8.0±2.6	1	+123.6±15.0	1	11.4	5.5	18.8	+108±033	-435±143	+037±058	+1724±805	-3855±2606
21	AW Lyn	0.080±0.003	-1.2±1.1	-4.2±1.9	1	+93.0±30.0	3	12.5	6.2	19.8	+142±044	-217±111	-047±060	+2048±1087	-41±2092
22	AX Lyn	0.026±0.001	+3.4±1.4	-2.0±2.8	1	38.5	18.9	45.6
23	AY Lyn	0.055±0.003	+1.2±1.4	-6.0±1.2	1	18.2	9.0	25.4
24	P 54-13	0.130±0.011	+2.6±1.0	-10.1±1.1	1	+069.0±10.0	2	7.7	3.9	15.2	+044±021	-374±051	+061±032	+1046±404	-2273±801
25	AZ Lyn	0.063±0.003	+3.3±1.0	-4.6±1.5	1	+087.0±33.0	3	15.9	8.1	23.1	-012±050	-374±114	207±070	+4933±1673	-3328±2492
26	BB Lyn	0.058±0.003	-0.6±0.7	-6.5±1.4	1	+058.0±33.0	3	17.2	8.9	24.4	+136±044	-505±118	-083±054	+4183±1429	-6557±2752
27	BC Lyn	0.053±0.003	+3.3±1.2	-3.1±0.7	1	+239.0±45.0	3	18.9	10.0	26.0	+075±068	-308±067	+345±091	+7628±2718	-2159±1627
28	AF 194	0.088±0.002	+0.5±0.8	-4.7±1.3	1	11.4	6.0	18.6
29	AF 197	0.105±0.003	-1.0±3.9	-8.2±1.8	1	9.5	5.0	16.9
30	DQ Lyn	0.649±0.043	-1.9±0.8	-28.7±1.0	2	+053.0±10.0	2	1.5	0.9	9.3	+047±009	-202±016	-006±008	+106±61	+167±144
31	RR7 032	0.163±0.004	-1.4±1.1	-11.9±1.1	1	+42.0±10.0	2	6.1	3.6	13.5	+069±020	-334±033	-039±026	+902±330	-1470±432
32	RR7 034	0.112±0.002	+0.1±0.7	-2.9±0.7	1	+316.0±10.0	2	8.9	5.2	16.1	+249±019	-130±030	+178±025	+1519±427	+1474±459
33	P 81 129	0.164±0.003	-0.5±2.0	-7.3±0.9	1	+003.0±10.0	2	6.1	3.6	13.4	+022±035	-204±026	-019±047	+648±477	+198±336
34	AF Lyn	0.079±0.002	+1.2±0.9	-5.9±1.0	1	-121.7±15.0	1	12.7	7.5	19.7	-132±034	-354±061	-036±044	+1462±557	-2444±1102
35	P 82 06	0.190±0.003	+4.0±3.0	-3.0±3.0	3	-211.0±10.0	2	5.3	3.3	12.6	-234±047	-84±075	-045±059	+919±470	+1684±903
36	AI Lyn	0.049±0.003	-1.5±1.2	-0.2±2.0	1	20.4	12.5	27.2
37	AK Lyn	0.084±0.004	+0.8±1.2	-8.7±1.1	1	+237.6±15.0	1	11.9	7.4	18.8	+157±044	-495±067	148±054	+2656±783	-4686±1203
38	RR7-079	0.260±0.007	+1.0±1.1	-13.5±1.2	1	-032.0±10.0	2	3.8	2.4	11.3	-047±015	-238±023	-021±017	+209±137	-212±253
39	RR7-086	0.073±0.005	-0.7±1.1	-4.0±0.7	1	13.7	8.5	20.6
40	AL Lyn	0.066±0.005	+1.0±0.8	-5.6±1.2	1	-065.8±15.0	1	15.2	9.5	22.0	-105±038	-398±087	-011±046	+2273±932	-3595±1789

Table 7. Continued.

No	ID	Π (mas)	μ_α (mas y ⁻¹)	μ_δ (mas y ⁻¹)	S_μ	RV (km s ⁻¹)	S_{RV}	D (kpc)	Z (kpc)	R_{gal} (kpc)	U (km s ⁻¹)	V (km s ⁻¹)	W (km s ⁻¹)	L_\perp (kpc km s ⁻¹)	L_z (kpc km s ⁻¹)
(1)	(2)	(3)	(4)	(5)	(6)	(7)	(8)	(9)	(10)	(11)	(12)	(13)	(14)	(15)	(16)
41	AM Lyn	0.045±0.002	+2.7±1.0	-3.7±1.3	1	22.2	13.9	28.9
42	P 82-32	0.122±0.004	+5.9±0.7	-9.5±1.6	1	+060.0±10.0	2	8.2	5.2	15.2	-084±019	-377±065	+213±022	+3615±414	-2219±931
43	AF 316	0.078±0.002	+1.9±1.1	-4.8±1.5	1	12.8	8.1	19.7
44	RR7-101	0.077±0.003	+0.5±1.0	-4.8±1.2	1	13.0	8.2	19.8
45	TT Lyn	1.408±0.029	-81.9±1.5	-41.8±0.9	2	-065.0±05.0	5	0.7	0.5	8.5	+132±006	-131±004	-240±007	+2108±62	+751±36
46	AF 400	0.184±0.011	+0.2±1.3	-8.5±1.4	1	5.4	3.8	12.4
47	AF 430	0.132±0.003	-1.4±1.1	-8.2±0.8	1	7.6	5.5	14.3
48	BS 16927-123	0.289±0.007	-15.6±2.4	-4.6±1.3	1	+070.0±10.0	2	3.5	2.6	10.6	+223±029	-094±022	-100±026	+1654±327	+1295±220
49	X LMi	0.437±0.007	+7.8±1.3	-17.3±0.7	2	-082±20.0	6	2.3	1.8	9.5	-152±016	-165±008	+004±018	+345±144	+507±78
50	AG UMa	0.104±0.002	-1.6±1.0	-8.4±1.9	1	9.6	8.4	15.2
51	BK UMa	0.348±0.013	-13.0±1.5	-16.9±2.2	1	+171.4±05.0	7	2.9	2.5	9.7	+174±019	-253±031	+120±012	+692±159	-341±292
52	AK UMa	0.075±0.002	-3.7±6.1	-3.3±6.3	1	13.3	11.8	18.5
53	AO UMa	0.096±0.003	-2.8±1.3	-6.3±1.3	1	10.4	9.4	15.6
54	BN UMa	0.248±0.006	+12.5±1.3	-17.3±1.7	1	+019.0±10.0	2	4.0	3.7	10.3	-306±024	-223±033	+175±014	+2810±223	+45±316
55	CK UMa	0.201±0.003	-3.8±1.3	+0.8±2.4	1	+016.0±10.0	2	5.0	4.9	10.2	+080±037	-018±053	+004±013	+1073±285	+1817±479

Notes to table:

(1) Sources of proper motions (S_μ): (1) GSCII-SDSS (2) Nomad (3) SDSS (DR 7)

(2) Sources of Radial Velocities (S_{RV}): (1) Pier, Saha, Kinman (2003); (2) Kinman, Brown (2010); (3) Saha, Oke (1984); (4) Pier (unpublished); (5) Fernley & Barnes (1997); (6) Layden (1994); (7) Jeffery et al. (2007).

(3) Distances: (D) Heliocentric distance; (Z) Height above Plane; R_{gal} Galactocentric distance assuming Solar Galactocentric Distance = 8.0 kpc

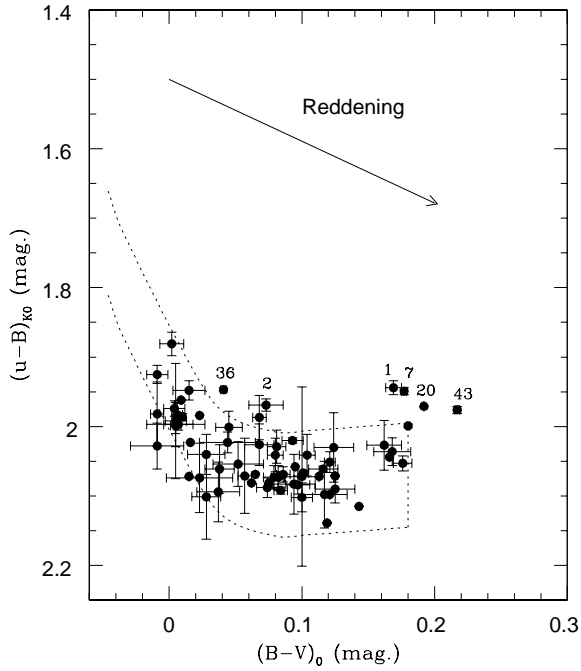


Figure A1. The ordinate $(u - B)_{K0}$ is defined in Kinman et al. (1994). The abscissa is Johnson $(B - V)_0$. The running numbers of stars in Table 1 are shown next to stars whose error bars lie outside the zone outlined by the dotted lines in which the BHB stars are located.

APPENDIX A: THE BHB STARS.

A1 Our Selection Methods.

Kinman et al. (1994) used both photometric and spectroscopic criteria to identify 15 BHB stars in the Anticentre field RR VII ($l = 183^\circ$, $b = +37^\circ$) which Kinman et al. (1982) had previously searched for RR Lyrae stars. Brown et al. (2003) independently confirmed these classifications for nine stars in this field (6 BHB and 3 non-BHB stars). The classification of these 15 stars (RR 7-02, -08, -15, -21, -23, -36, -43, -53, -58, -60, -64, -66, -84, -90, -91)⁶ is therefore considered to be secure.

Additional BHB star *candidates* with $(170^\circ < l < 207^\circ)$ were taken from BHB candidates discovered in the objective prism surveys of Pesch & Sanduleak (1989) (AF-nnn) and Beers et al. (1996) (BS nnnnn-nnn). We also included unpublished BHB candidates from the Case Survey that were kindly made available to us by Dr Peter Pesch; we call these P nn.nn stars. All these stars are included in Table 4 (main section of this paper) with a running number which is also used as a means of identification in the figures.

Following Kinman & Brown (2011), BHB stars were selected from these *candidates* by 3 methods:

(a) The $(u - B)_{K0}$ vs. $(B - V)_0$ plot where u is a Strömgren magnitude and B and V are Johnson magnitudes. The plot is shown in Fig. A1 where the dotted lines enclose an area in which $(B - V)_0 \leq 0.18$ and $(u - B)_{K0}$ is within ± 0.075 mag of a curve defined

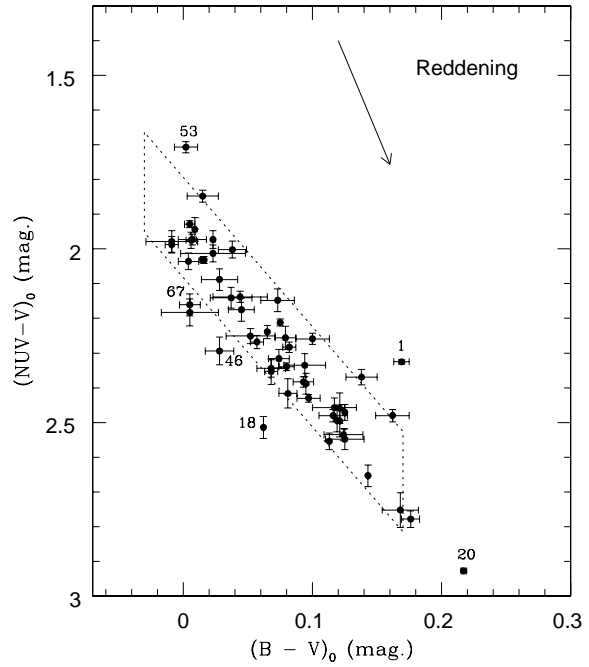


Figure A2. The ordinate is the de-reddened difference between the *GALEX* *NUV* magnitude (effective wavelength 2267 Å) and the Johnson V magnitude. The abscissa is the Johnson $(B - V)_0$ colour. The dotted parallelogram is the expected location of BHB stars according to Kinman et al. (2007). The running numbers of stars in Table 1 whose error bars lie outside this parallelogram are shown next to these stars.

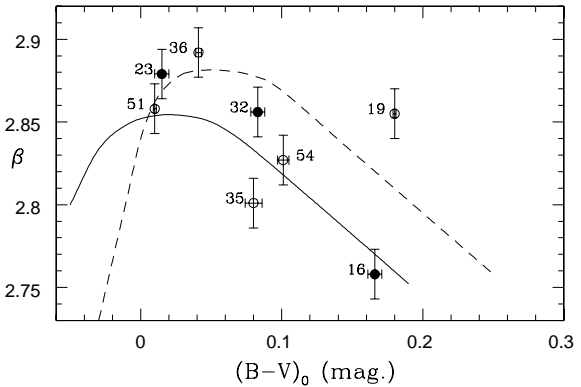


Figure A3. The ordinate is Strömgren β and the abscissa is Johnson $(B - V)_0$. The solid curve shows the location of BHB stars; the dashed curve shows the lower limit of β for non-BHB stars. Further details are given in Kinman & Brown (2011).

by nearby BHB stars whose classification rests on high-resolution spectroscopy (Kinman et al. 2000; Behr 2003).

(b) The $(NUV - V)_0$ vs. $(B - V)_0$ plot where NUV is the near-UV *GALEX* magnitude (effective wavelength 2267 Å) taken from the *MAST* (Multimission Archive at STScI, <http://archive.stsci.edu/>). The plot is shown in Fig. A2 where the dotted parallelogram (taken from Kinman et al. 2007a) shows the expected location of BHB stars. This method can only be used for

⁶ The identifications [KSK94]RR 7 nnn, Case A-F nnn and BPS BS nnnnn-nnn used by *SIMBAD* are abbreviated in this paper to RR7-nnn, AF-nnn and BS nnnnn-nnn respectively.

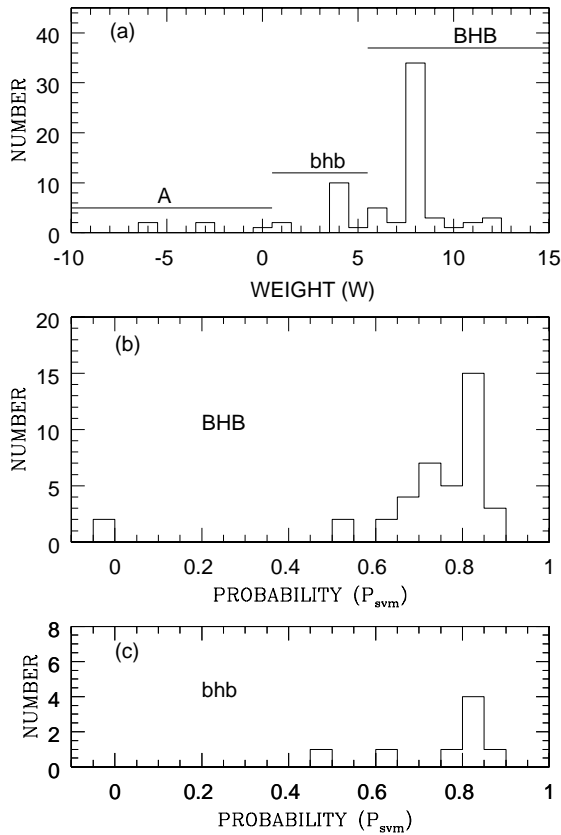


Figure A4. (a) Frequency distribution of the weights given to the program stars: the more positive the weight, the greater the probability that the star is a BHB star. Stars with weights greater or equal to 6 are classified as BHB stars. Stars with weights of zero or less are classified as A stars. Stars of intermediate weight are given the intermediate classification of bhb. (b) Frequency distribution of the probability (P_{svm}) that a star classified as BHB is a BHB star. (c) Frequency distribution of the probability (P_{svm}) that a star classified as bhb is a BHB star. P_{svm} is described in the text.

stars fainter than about $V = 12$ because the *GALEX* magnitudes of brighter stars are affected by saturation.

(c) The Strömgen β vs. $(B - V)_0$ plot is shown in Fig. A3 which is taken from Fig 9(a) of Kinman & Brown (2011). The full curve shows the expected location of BHB stars and dashed curve shows the lower limit of β for non-BHB stars. This method was only used for 8 of the brighter stars.

In these figures, a running number (from Table 1) is given against each star in Fig. A3 and for those stars whose error bars lie outside the defining boxes in Figs. A1 & A2. For stars in (a) Fig. A1 and (b) Fig. A2, those whose colours fall within the defining box were given weight +4; those whose error bars intersected the defining box were given weight +2 and the rest were given weights of 0 or -3 according to their distance from the defining box. For the stars in (c) Fig. A3, those whose error bars intersect the full curve are given weight 3, those whose error bars lie above this line but below the dashed line are given weight 1 and those with larger β are given weight -3. The weights from the three methods were added to give a total weight (W) that is given in column 14 of Table 1. Stars with $W \geq 6$ are taken to have a high probability of being BHB stars; those with zero or negative weights are taken to have a high probability of not being a BHB star (class A) while those with

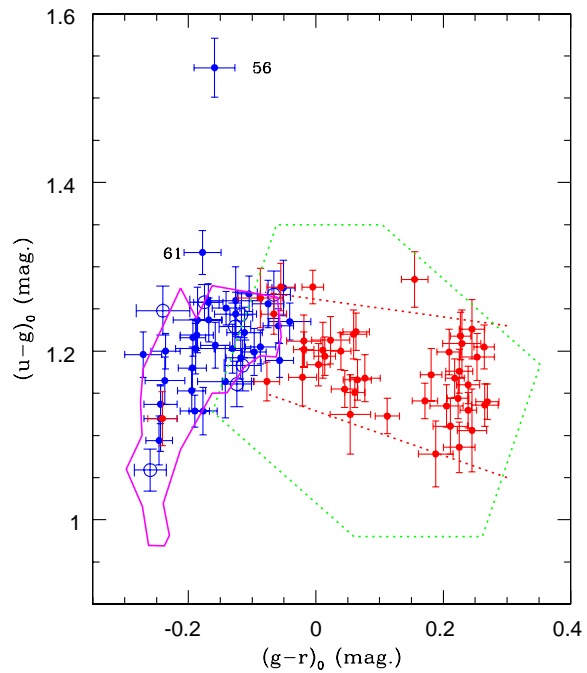


Figure A5. The ordinate is SDSS $(u - g)_0$ and the abscissa is $(g - r)_0$. Stars classified as BHB are shown as blue filled circles. Stars classified as bhb are shown as blue open circles. RR Lyrae stars are shown as red filled circles. The area enclosed by the magenta line is the locus of the BHB stars according to Ruhland et al. (2011). The green dotted hexagon is the locus of the RR Lyrae stars according to Watkins et al. (2009). The red dotted lines show our colour limits for the RR Lyrae stars.

intermediate W are considered to be an intermediate class which we call “bhb”. The distribution of these three classes as a function of the weight (W) is shown in Fig. A4 (a).

A2 Comparison with other Selection Methods.

Smith et al. (2010) have used machine-learning methods to estimate the probability that a star is a BHB star from its SDSS photometry. Their preferred probability (P_{svm}) is derived from the *support vector machine* method and is available for those of our program stars whose SDSS magnitudes are unsaturated (roughly those with $V > 14.5$). The distribution of P_{svm} for the stars that we classify as BHB and bhb are shown in Fig. A4(b) and Fig. A4(c) respectively. Most of the stars that we classify as BHB and bhb have a high probability of being BHB stars on the Smith et al. criterion. The only exception is our program star 47 (BS 16468-00260) which is missing from the Smith et al. (2010) catalogue although its $(u - g)_0$ and $(g - r)_0$ are similar to those of stars that are given a high value of P_{svm} . The stars that we classify as bhb all have P_{svm} greater than 0.6; this suggests that most are likely to be BHB stars.

Ruhland et al. (2011) have shown that the BHB stars lie in a relatively well-defined locus in the $(u - g)_0$ vs. $(g - r)_0$ diagram; this is enclosed by the full magenta line in Fig. A5. All the stars with unsaturated SDSS magnitudes that we classify as BHB or bhb (shown by filled blue circles and blue open circles respectively) lie within this line except for stars 56 and 61 for which we assigned weights +11 and +8 respectively. There are two discrepant u mag-

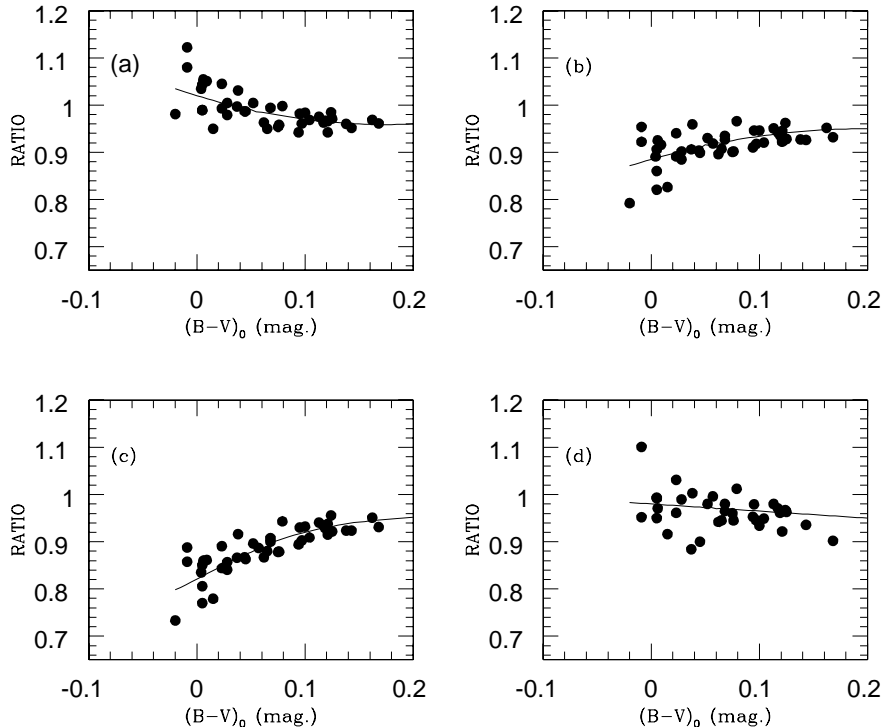


Figure A6. The ordinate is the ratio of the distance of a star by a given method divided by the distance (D2) for the same star as a function of $(B - V)_0$. (a) Distances D1 given by Smith et al. (2010). (b) Distances (D3) derived from the cubic in $(B - V)_0$ given by Preston et al. (1991). (c) Distances D4 are derived from the cubic fit in $(B - V)_0$ for M3 and M13. (d) Distances (D5) derived from a cubic fit in $(V - K)_0$. For further details see text.

nitudes for the object in the position of star 56 and this presumably explains the location of this star in Fig. A5. Star 61 has $V = 14.57$ which is close to the saturation limit of SDSS magnitudes. For these reasons we think that the anomalous locations of stars 56 and 61 are caused by errors in the SDSS magnitudes and that the high weights that we have assigned to these stars are trustworthy. Overall, there is satisfactory agreement between our selection criteria and the most recent selection criteria based on SDSS magnitudes.

A2.1 Reddenings

The reddenings $E(B - V)$ in this paper were taken from the total reddenings of Schlegel et al. (1998). All but 5 of our BHB and RR Lyrae stars are more than 1 kpc above the galactic plane and so the reddenings to these stars will be close to the total reddenings in these sight-lines. The reddening corrections for other colours are derived from the relations $E(V - K) = 2.75E(B - V)$, $A_V = 3.1E(B - V)$ and $A_K = 0.35E(B - V)$ (Cardelli et al. 1989).

A3 Distances of the BHB stars.

We have used five methods to determine absolute magnitudes (and hence distances) for our BHB stars.

(1) Sirko et al. (2004) gave absolute SDSS g magnitudes based on models by Dorman et al. (1993) for various BHB properties including SDSS colours. Smith et al. (2010) used this data to derive distances for their sample of BHB stars which includes 40 of our BHB and bhb stars; these are given as D1 in Table A1.

(2) Deason et al. (2011) derived the absolute magnitudes of

BHB stars from the SDSS photometry of 11 globular clusters by An et al. (2008). They expressed the absolute magnitude (M_g) in their equation (7) as a quartic in $(g - r)_0$. We used this expression to derive distances (D2 in Table A1) for the 43 stars for which unsaturated SDSS colours were available from SDSS DR7⁷.

(3) Preston, Schectman and Beers (1991) used the Johnson photometry of 15 globular clusters to derive the absolute V magnitude of BHB stars in terms of a cubic in $(B - V)_0$. A slightly adjusted version of this expression is given as their equation (5) by Kinman et al. (2007b). We used this expression to derive the distances (D3) in Table A1.

(4) Kinman et al. (2007b) attempted to improve on the cubic equation in (c) by deriving another cubic based on the photometry of the intermediate-metallicity globular clusters M3 (Ferraro et al. 1997) and M13 (Paltrinieri et al. 1998). This cubic is given as their equation (6) in Kinman et al. (2007b). The corresponding distances are given as (D4) in Table A1.

(5) Kinman et al. (2007b) gave a cubic expression for the infrared absolute magnitude M_K in terms of the $(V - K)_0$ colours. The calibration was derived from the colour magnitude diagrams of the globular clusters M3 and M13 given by Valenti et al. (2004). This cubic is given as their equation (3) by Kinman et al. (2007b). The corresponding distances are given as (D5) in Table A1.

Methods (1) and (2) are only available for the stars with unsaturated SDSS magnitudes (roughly $V > 14.5$). Methods (3) and (4) are possible for all stars in the sample while method (e) is only used

⁷ This expression gives ($M_g \sim 0.44$ at the blue edge of the instability gap; this corresponds to $M_V \sim 0.58$).

for the brighter stars whose 2MASS K -magnitudes have errors less than 0.15 mag. We assume that the distances D2 are the most reliable because they are based on the recent homogeneous photometry of 11 globular clusters that have well established moduli. For each star, and for each method, we have computed a ratio F that equals the distance for that method divided by its distance D2. These ratios are plotted for each method as a function of $(B - V)_0$ in Fig. A6. The values of F for distances D4 (Fig 6(c)) are always less than those for D3 (Fig 6(b)). This shows that method (4) is inferior to method (3) in determining M_V as a function of $(B - V)_0$; the distances D4 are therefore not considered further. Smoothed curves were fitted to the plots in Fig A6 (a), (b) and (c) and these have the following analytic expressions as a function of $(B - V)_0$:

$$F1 = 1.020 - 0.700(B - V)_0 + 2.000(B - V)_0^2 \quad (D1)$$

$$F2 = 1.000 \quad (D2)$$

$$F3 = 0.885 + 0.655(B - V)_0 - 1.650(B - V)_0^2 \quad (D3)$$

$$F5 = 0.980 - 0.150(B - V)_0 \quad (D5)$$

Here, for example, the expression F1 is the quantity by which the distance D1 must be divided to get it onto the scale of the distances called D2. There is no F4 because we do not use the distance called D4. The distances D1, D2, D3 and D5 were then divided respectively by F1, F2, F3 and F5 to give the corrected distances d1, d2, d3 and d5. The adopted distance (D) is the unweighted mean of these corrected distances. All these distances are given in Table A1.

We assume that the random error in these distances is given by the rms scatter among the distances d1, d2, d3 and d5. This is given (in kpc) in col. 15 in Table A1. We have used these errors in computing the error bars of the velocities and angular momenta (L_\perp , L_z) that are distant-dependent. It remains to consider the effect of possible systematic errors. The point at issue is whether these systematic errors depend on distance. If they do, there would be systematic errors in our velocities and angular momenta that would produce errors in these quantities as a function of galactocentric distance. The most likely source of a distance-dependent error is in the absolute magnitudes and proper motions since neither the radial velocity, apparent magnitude or extinction are likely to have distance-dependent errors. Such an error could arise if the mean colours of our BHB stars varied with distance. Using only the stars that we used in our velocity and angular momentum analyses, we find a mean $(B - V)_0$ of $+0.61 \pm 0.018$, $+0.075 \pm 0.012$ and $+0.081 \pm 0.012$ mag at mean galactocentric distances of 10.6, 13.4 and 15.9 kpc respectively. These data would be compatible with a difference of say 0.02 magnitudes in the mean $(B - V)_0$ between galactocentric distances of 10.6 and 13.4 kpc. This corresponds to a difference in 0.05 mag in the absolute magnitude or 2.3% in the distance. This error is far too small to account for the change in galactic rotation (V) of about 100 km s^{-1} between these two distances. Likewise, it would require a *systematic difference* of -1.6 mas y^{-1} between the proper motions of the stars at $V = 13.0$ and those at $V = 15.0$ to produce the differences in galactic rotation (V) that we observe (Sec 5.2). This seems unlikely since the galactic U and W velocities show no dependence on distance.

APPENDIX B: RR LYRAE STARS.

B1 The new RR Lyrae stars.

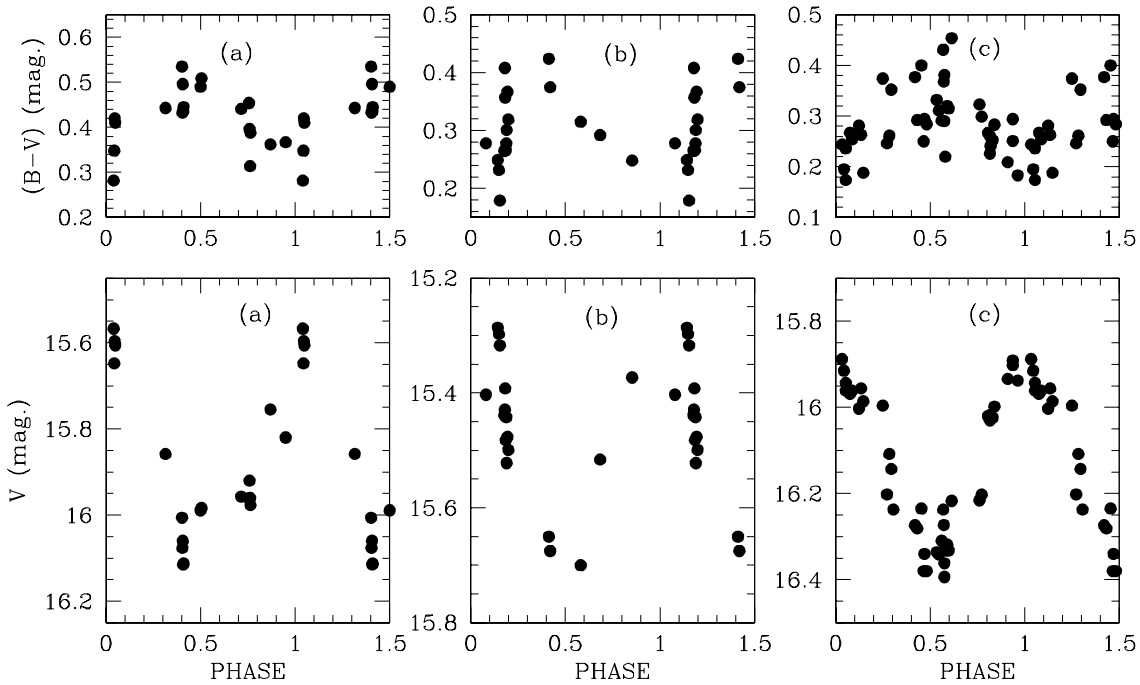
Seven of the stars listed in Table 5 (identified by a 7 in the Notes column) have not previously be identified as RR Lyrae stars. All are of low amplitude and all but one are of Bailey type *c*. Their V and $B - V$ light curves are given in Figs. B1 and B2. The ephemerides and photometric data for these variables are given in Table B1. The observations were made in the same way as those described by Kinman & Brown (2010) but in general there are fewer observations than for the stars observed in that paper. This is particularly true of AF-194, AF-197, AF-400 and AF-430. Consequently, the periods of these stars are less reliable than we would wish. In assigning periods and Bailey types, however, we took into account the mean $(B - V)$ colours which are well determined and which can be used to distinguish between Bailey type *c* and Bailey type *ab*. These Bailey types are therefore more certain than would be inferred from the V light-curves alone.

Table A1. Distances in kpc for BHB and bhb stars. The distances D1, D2, D3, D4 & D5 and the corrected distances d1, d2, d3 & d5 are defined in the text. The adopted distance D and its rms error σ are given in columns (14) and (15).

No	ID	Class	D1	D2	D3	D4	D5	$(B - V)_0$	d1	d2	d3	d5	D	σ
(1)	(2)	(3)	(4)	(5)	(6)	(7)	(8)	(9)	(10)	(11)	(12)	(13)	(14)	(15)
02	4-32.5	bhb	8.210	8.567	7.728	7.534	8.096	0.076	8.392	8.567	8.352	8.358	8.417	0.058
03	AF-186	BHB	9.450	9.602	9.081	8.948	8.972	0.100	9.742	9.602	9.723	9.279	9.591	0.119
04	AF-189	BHB	7.580	7.606	6.893	6.583	6.727	0.037	7.604	7.606	7.600	6.903	7.428	0.202
05	54-111	BHB	5.900	6.137	5.633	5.544	5.798	0.097	6.077	6.137	6.037	6.005	6.064	0.033
06	54-122	bhb	7.360	6.813	6.280	5.846	6.486	-0.009	7.170	6.813	7.145	6.609	6.934	0.156
08	54-119	BHB	5.166	5.158	5.134	0.176	5.443	5.384	5.413	0.042
09	17444-25	bhb	0.697	0.682	0.708	0.084	0.751	0.732	0.742	0.013
10	AF-209	BHB	13.670	13.822	11.343	10.640	...	0.005	13.447	13.822	12.770	...	13.346	0.377
11	AF-210	bhb	8.730	9.093	8.427	8.399	...	0.138	9.080	9.093	8.927	...	9.033	0.065
12	AF-214	BHB	9.810	10.206	9.514	9.504	9.209	0.168	10.231	10.206	10.031	9.645	10.028	0.156
13	RR7-02	BHB	7.530	7.912	7.326	7.307	7.402	0.143	7.837	7.912	7.753	7.722	7.806	0.050
14	81-42	BHB	5.290	5.349	4.598	4.313	5.080	0.005	5.204	5.349	5.177	5.188	5.230	0.046
15	RR7-08	BHB	7.510	7.871	7.093	6.911	7.559	0.075	7.673	7.871	7.669	7.803	7.754	0.058
16	RR7-15	BHB	1.606	1.605	1.608	0.166	1.694	1.684	1.689	0.007
17	81-39	BHB	9.710	9.383	8.361	7.839	...	0.004	9.546	9.383	9.420	...	9.450	0.060
18	RR7-21	bhb	8.210	8.525	7.637	7.393	8.027	0.062	8.341	8.525	8.308	8.269	8.361	0.065
19	81-72	bhb	1.678	1.676	1.633	0.174	1.768	1.712	1.740	0.040
21	RR7-23	BHB	2.057	1.941	2.235	0.015	2.300	2.286	2.293	0.010
22	RR7-36	BHB	7.940	8.426	7.772	7.714	7.766	0.121	8.232	8.426	8.267	8.074	8.250	0.083
23	81-101	bhb	9.050	9.323	8.652	8.597	8.980	0.125	9.390	9.323	9.194	9.342	9.312	0.048
24	81-121	BHB	9.650	11.366	8.393	7.916	9.304	0.015	9.555	11.366	9.383	9.516	9.955	0.545
25	RR7-043	BHB	14.950	14.222	13.028	12.247	...	0.009	14.746	14.222	14.626	15.880	14.868	0.410
26	28-45	bhb	5.041	4.967	5.171	0.100	5.397	5.359	5.378	0.027
27	RR7-053	BHB	7.340	7.593	7.107	7.050	7.294	0.119	7.606	7.593	7.564	7.581	7.586	0.010
28	81-162	BHB	11.580	11.735	10.614	10.176	...	0.044	11.661	11.735	11.656	...	11.684	0.031
29	RR7-058	BHB	8.410	8.051	7.571	7.174	8.298	0.023	8.369	8.051	8.420	8.497	8.334	0.113
30	RR7-60	BHB	5.565	5.530	5.698	0.125	5.913	5.928	5.920	0.011
31	82-04	BHB	10.390	10.345	9.327	8.863	...	0.028	10.370	10.345	10.340	...	10.352	0.016
32	RR7-64	BHB	1.195	1.169	1.223	0.083	1.288	1.264	1.276	0.017
33	RR7-66	BHB	8.220	8.372	7.917	7.785	8.193	0.095	8.461	8.372	8.492	8.484	8.452	0.032
34	81-167	BHB	5.192	5.057	5.438	0.074	5.616	5.613	5.614	0.002
35	11419-01	BHB	2.416	2.360	2.486	0.080	2.607	2.568	2.588	0.028
37	AF-293	BHB	13.090	13.513	12.864	12.852	...	0.162	13.648	13.513	13.572	...	13.578	0.048
38	11419-04	BHB	6.580	6.242	5.772	5.371	6.061	0.006	6.477	6.242	6.494	6.190	6.351	0.091
39	RR7-84	BHB	10.250	10.509	9.990	9.891	10.300	0.113	10.606	10.509	10.651	10.695	10.615	0.046
40	RR7-91	BHB	4.257	4.017	4.629	0.016	4.756	4.735	4.746	0.015
41	RR7-90	BHB	9.540	10.042	9.113	8.836	9.486	0.065	9.705	10.042	9.899	9.777	9.856	0.085
42	82-49	BHB	8.780	8.798	8.497	8.296	8.907	0.079	8.985	8.798	9.172	9.200	9.039	0.108
44	16473-102	BHB	4.223	4.129	4.373	0.082	4.553	4.519	4.536	0.024
45	17139-69	BHB	5.650	5.847	5.523	5.482	5.635	0.121	5.857	5.847	5.875	5.859	5.867	0.011
46	TON 384	bhb	7.920	8.089	7.157	6.801	8.011	0.028	7.904	8.089	7.934	8.210	8.034	0.082
47	16468-26	BHB	...	6.436	5.913	5.709	6.410	0.057	...	6.436	6.448	6.598	6.494	0.064
48	AF-379	BHB	8.200	8.310	7.473	7.168	7.476	0.045	8.262	8.310	8.202	7.681	8.114	0.168
49	AF-386	BHB	7.280	7.324	6.848	6.650	7.068	0.068	7.416	7.324	7.428	7.288	7.364	0.040
50	AF-390	BHB	8.470	8.533	7.599	7.200	8.204	0.023	8.428	8.533	8.451	8.401	8.453	0.033
51	16468-78	BHB	1.361	1.280	1.498	0.010	1.527	1.531	1.529	0.003
52	30-16	bhb	5.650	5.830	5.369	5.298	5.531	0.104	5.832	5.830	5.741	5.735	5.784	0.018
53	16468-80	bhb	4.043	3.786	4.297	0.002	4.562	4.386	4.474	0.124
54	30-28	BHB	0.804	0.793	0.831	0.101	0.861	0.861	0.861	0.000
55	16468-90	BHB	4.743	4.700	4.771	0.116	5.052	4.956	5.004	0.068
56	CHSS 608	BHB	...	6.728	6.237	6.057	6.593	0.068	...	6.728	6.765	6.798	6.764	0.025
57	11424-28	BHB	5.470	5.345	5.727	0.081	5.899	5.917	5.908	0.013
58	30-038	BHB	5.570	5.655	5.440	5.404	5.466	0.124	5.778	5.655	5.782	5.685	5.725	0.037
59	57-121	BHB	8.220	8.381	6.641	6.146	...	-0.020	7.944	8.381	7.622	...	7.982	0.269
60	AF-419	BHB	7.930	8.416	7.655	7.524	8.017	0.094	8.160	8.416	8.214	8.300	8.272	0.157
61	11424-070	BHB	5.920	5.896	5.483	5.280	5.776	0.052	5.986	5.896	5.995	5.941	5.954	0.026
62	16927-22	bhb	1.202	1.177	1.251	0.086	1.294	1.294	1.294	0.000
63	CHSS 663	BHB	7.680	7.446	7.140	6.822	7.469	0.038	7.709	7.446	7.868	7.666	7.672	0.100
64	11424-82	BHB	7.280	7.558	7.122	7.060	7.338	0.117	7.540	7.558	7.584	7.624	7.576	0.021
65	16940-45	BHB	3.217	3.021	3.551	0.007	3.617	3.627	3.622	0.007
66	16927-55	BHB	5.770	5.141	4.902	4.563	5.659	-0.009	5.621	5.141	5.577	5.767	5.526	0.156
67	16940-70	bhb	7.160	6.864	6.216	5.831	6.810	0.005	7.043	6.864	6.998	6.954	6.965	0.044
68	16940.72	BHB	4.433	4.356	4.586	0.093	4.758	4.747	4.752	0.008

Table B1. Ephemerides and Photometric Data for the Seven New RR Lyrae Stars.

Star	Type	Period (days)	JD _{max} 24000+	$\langle V \rangle$ (mag)	V_{amp} (mag)	$\langle (B - V) \rangle$ (mag)
AF-194	<i>ab</i>	0.8410:	49736.740	15.85	0.45	0.40
AF-197	<i>c</i>	0.38802	49416.650	15.50	0.40	0.30
RR7-086	<i>c</i>	0.353878	47538.525	16.14	0.63	0.29
AF-316	<i>c</i>	0.3455178	49010.793	16.13	0.46	0.28
RR7-101	<i>c</i>	0.329836	47538.685	16.15	0.60	0.22
AF-400	<i>c</i>	0.403114	50503.429	14.10	0.40	0.20
AF-430	<i>c</i>	0.30517	50503.723	14.90	0.40	0.22

**Figure B1.** The V and $(B - V)$ light curves for the RR Lyrae variable: (a) AF-194, (b) AF-197 and (c) AF-316. Further information on these stars is given in Table B1.**B2 The Distances of the RR Lyrae stars.**

We use three methods to estimate the distances of our RR Lyrae stars; details of these methods are given in Kinman et al. (2007b).

(1) The absolute visual magnitude M_V is derived in terms of the metallicity $[Fe/H]$ using coefficients given by Clementini et al. (2003):

$$M_V = 0.214[Fe/H] + 0.86$$

If $[Fe/H]$ is not known, it is assumed to -1.6 . An error of ± 0.5 dex in $[Fe/H]$ leads to an error of ± 0.1 mag in the distance modulus and about 5% in the parallax.

(2) The infrared absolute magnitude (M_K) is derived from $[Fe/H]$ and the Period (P) (in days) in the form given by Nemeč et al. (1994):

$$M_K = -2.40 \log P + 0.06[Fe/H] - 1.06$$

The periods of the Bailey type *c* stars must be “fundamentalized”. For this purpose, we assumed that the ratio of the period of the

first overtone (*c* type) to that of the fundamental (*ab* type) is 0.745 (Clement et al., 2001).

(3) The infrared magnitude (M_K) can be derived from $(V - K)_0$ and the metallicity $[Fe/H]$:

$$M_K = 1.166 + 0.18[Fe/H] - 1.812(V - K)_0 + 0.675(V - K)_0^2 - 0.183(V - K)_0^3$$

If $[Fe/H]$ is not known, it is assumed to be -1.6 . In this case the relation is the same as that used in method (5) for the BHB stars.

In a recent review, Feast (2011) has shown that the current calibration of RR Lyrae absolute magnitudes is not satisfactory: there is a significant spread in the coefficients and zero points derived from trigonometric parallaxes, statistical parallaxes and pulsation parallaxes. It is hoped that, in the future, new trigonometric parallaxes such as those recently given by Benedict et al. (2011) will eventually improve this situation. The expressions for the RR Lyrae absolute magnitudes given above are the best that we have available now but may well require some correction in the future.

Table B2. Distance estimates of RR Lyrae stars. Adopted distance is D.

No.	Star	D_a (kpc)	D_b (kpc)	D_c (kpc)	d_a (kpc)	d_b (kpc)	d_c (kpc)	D (kpc)	error (kpc)
1	V385 Aur	22.163	22.738	22.74	1.14
2	V386 Aur	16.362	16.786	16.79	0.84
3	V387 Aur	17.131	17.575	17.58	0.88
4	V389 Aur	23.288	23.892	23.89	1.19
5	VX Lyn	18.293	18.767	18.77	0.94
6	VY Lyn	10.157	9.851	9.972	10.420	9.875	10.464	10.25	0.23
7	VZ Lyn	12.527	12.852	12.85	0.64
8	WX Lyn	17.347	17.797	17.80	0.89
9	AS Lyn	33.035	33.891	33.89	1.69
10	WZ Lyn	5.352	5.674	5.230	5.491	5.688	5.488	05.56	0.08
11	XZ Lyn	13.473	13.822	13.82	0.69
12	TW Lyn	1.644	1.651	1.644	1.687	1.655	1.725	01.69	0.02
13	YY Lyn	7.307	7.566	7.087	7.496	7.584	7.437	07.51	0.05
14	YZ Lyn	20.675	21.211	21.21	1.06
15	AU Lyn	27.497	28.210	28.21	1.41
16	ZZ Lyn	10.448	12.344	10.102	10.719	12.374	10.600	11.23	0.07
17	RW Lyn	2.810	2.598	2.761	2.883	2.604	2.897	02.79	0.12
18	AV Lyn	15.668	16.074	16.07	0.80
19	AC Lyn	13.774	14.131	14.13	0.71
20	AD Lyn	10.536	12.494	10.144	10.809	12.524	10.644	11.33	0.74
21	AW Lyn	12.594	11.718	12.363	12.921	11.746	12.973	12.55	0.49
22	AX Lyn	37.560	38.534	38.53	1.92
23	AY Lyn	17.562	18.017	18.02	0.90
24	P 54-13	7.953	6.648	7.797	8.159	6.664	8.182	07.67	0.63
25	AZ Lyn	15.465	15.866	15.87	0.79
26	BB Lyn	16.922	17.361	17.36	0.87
27	BC Lyn	18.481	18.960	18.96	0.95
28	AF 194	10.832	11.637	10.615	11.113	11.665	11.139	11.31	0.22
29	AF 197	9.396	9.177	9.223	9.640	9.199	9.678	09.51	0.19
30	DQ Lyn	1.416	1.707	1.387	1.453	1.711	1.455	01.54	0.10
31	RR7 032	6.072	5.963	5.955	6.229	5.977	6.249	06.15	0.11
32	RR7 034	8.636	9.103	8.314	8.860	9.125	8.724	08.90	0.14
33	P 81 129	5.954	6.030	5.802	6.108	6.045	6.088	06.08	0.02
34	AF Lyn	12.433	12.253	12.209	12.755	12.282	12.811	12.62	0.21
35	P 82 06	5.148	5.223	4.984	5.281	5.236	5.230	05.25	0.02
36	AI Lyn	19.799	20.312	20.31	1.02
37	AK Lyn	11.917	11.033	11.706	12.226	11.060	12.283	11.86	0.49
38	RR7-079	3.809	3.688	3.735	3.908	3.697	3.919	03.84	0.09
39	RR7-086	12.779	15.001	12.274	13.110	15.037	12.879	13.68	0.84
40	AL Lyn	15.546	13.419	15.173	15.949	13.451	15.921	15.11	1.01
41	AM Lyn	21.678	22.240	22.24	1.11
42	P 82-32	7.785	8.543	7.592	7.987	8.564	7.966	08.17	0.24
43	AF 316	12.757	12.218	12.519	13.088	12.247	13.136	12.82	0.35
44	RR7-101	12.967	12.239	12.723	13.303	12.268	13.350	12.97	0.43
45	TT Lyn	0.699	0.694	0.689	0.717	0.696	0.723	00.71	0.01
46	AF 400	5.074	5.915	4.929	5.206	5.929	5.172	05.44	0.30
47	AF 430	7.355	7.697	7.127	7.546	7.716	7.478	07.58	0.09
48	16927-123	3.326	3.547	3.248	3.412	3.556	3.408	03.46	0.06
49	X LMi	2.224	2.293	2.188	2.282	2.299	2.296	02.29	0.01
50	AG UMa	9.398	9.453	9.205	9.642	9.476	9.659	09.59	0.07
51	BK UMa	2.869	2.704	2.825	2.943	2.711	2.964	02.87	0.10
52	AK UMa	12.736	13.915	12.503	13.066	13.948	13.120	13.38	0.35
53	AO UMa	9.890	10.806	9.692	10.146	10.832	10.170	10.38	0.28
54	BN UMa	3.871	4.136	3.794	3.971	4.146	3.981	04.03	0.07
55	CK UMa	4.984	4.686	4.886	5.113	4.697	5.127	04.98	0.17

Distances D_a , D_b and D_c were derived for our RR Lyrae stars using methods (1), (2) and (3) respectively and are given in Table B2. There are 31 of these RR Lyrae stars that have both radial velocities and proper motions and that are closer than 17 kpc (the limit that we have taken for the proper motions to yield meaningful velocities). Of these 31 stars, 19 have known $[\text{Fe}/\text{H}]$ and 26 have K magnitudes. As noted above, distances can be derived even if $[\text{Fe}/\text{H}]$ is not known by assuming that it is -1.6 , although this involves a loss of accuracy. We need the distances of the RR Lyrae stars to be as closely as possible on the same scale as that of the BHB stars. Now method (3) for the RR Lyraes (with $[\text{Fe}/\text{H}] = -1.6$) is the same as method (5) for the BHB stars (with $(B - V)_0 = +0.18$). We have therefore converted the distances D_a and D_b to the scale of the distances D_c by dividing them by the factors R_a and R_b respectively. R_a is the mean value of D_a/D_c and equals 1.0228 ± 0.0005 . R_b is the mean value of D_b/D_c and equals 1.0468 ± 0.0017 . After we have divided the distances D_a by 1.0228 and the distances D_b by 1.0468, they will be on the scale of D_c which is the same as the BHB scale D_5 . Now the BHB stars were all adjusted to be on the scale of BHB distance D_2 . To get the RR Lyrae star's distances on this scale, they must further be divided by the factor F_5 (see Sec. A3). This factor (F_5) must be evaluated at the blue edge of the instability gap ($(B - V)_0 = +0.18$) where it has the value 0.953. We call the final values of these RR Lyrae distances d_a , d_b and d_c . All these distances and our adopted distance (D) which is the unweighted mean of d_a , d_b and d_c are given in Table B2.

For the 35 RR Lyrae stars where all three distances are available, our adopted distance is the arithmetic mean of the three distances and σ is the *rms* scatter of a single distance. In Fig. B3 we have plotted σ/D against D for (a) the 9 stars for which $[\text{Fe}/\text{H}]$ and $\langle K \rangle$ are best determined and (b) for the remaining 26 stars for which σ is available. We see that σ/D is roughly independent of distance and less than 0.06 except for the 7 numbered stars in Fig B3(b). It seems likely that the larger σ/D of these stars is produced by larger errors in $\langle K \rangle$. In the cases where only d_a is available we therefore conservatively adopted $\sigma = 0.05 D$ for its error. Some allowance must be made for systematic errors in our distance scale and this can only be a rough estimate based on the spread amongst the various distance estimates that we have used. In calculating the space motions we have included a systematic error of $0.015 D$ in quadrature with the random errors given in Tables A1 and B2.

Our distances for TT Lyn, TW Lyn and X LMi (0.71 ± 0.01 ; 1.69 ± 0.02 ; 2.20 ± 0.01 kpc) are in satisfactory agreement with those given in the recent compilation of bright RR Lyrae stars by Maintz (2005) (0.71 ; 1.65 ; 2.20 kpc).

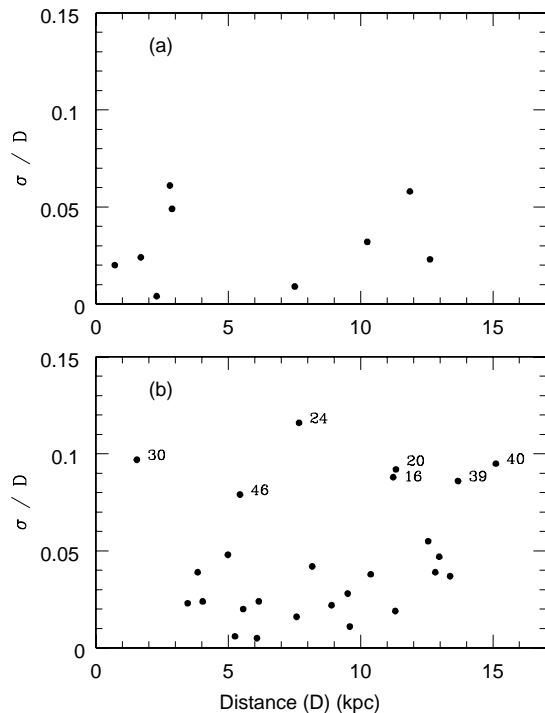


Figure B3. The *rms* scatter (σ) in distance estimates divided by the adopted distance (D) in kpc (ordinate) *vs* D (abscissa). (a) Nine stars with best determined $[\text{Fe}/\text{H}]$ and $\langle K \rangle$. (b) Twenty six remaining stars for which σ is available. The numbers identify the stars in Table 2. Further information on these stars see text.

APPENDIX C: PROPER MOTIONS

The proper motions used in this paper come from astrometric data that were assembled from the Second Guide Star Catalog (GSC-II) Lasker et al. (2008) and the Seventh Data Release of the Sloan Digital Sky Survey SDSS DR7 Abazajian et al. 2009; Yanny et al. 2009). Absolute proper motions were obtained by correcting the relative proper motions to a reference frame provided by a Large Quasar Reference Frame assembled by Andrei et al. (2009). Proper motions were computed for 77 million sources by combining SDSS second-epoch positions with multi epoch positions derived from the GSC-II database and spanning a time baseline of 40 to 50 years. As described in Spagna et al. (2010), proper motion formal errors are typically in the range 2 to 3 mas y^{-1} at intermediate magnitudes ($16 < r < 18.5$). Comparisons against a sample of 80 000 QSO indicate that the random errors of the two catalogues are, on average, comparable but that the reference system of the SDSS proper motions is affected by a global systematic rotation $\Delta\mu \simeq -0.40 \text{ mas y}^{-1}$, which is not present in the GSC-II frame. Further details concerning the data base from which our proper motions were obtained may be found in Spagna et al. (2010a; 2010b).

Overall, we consider these proper motions to be the most accurate available for the magnitude range, $14 \lesssim V \lesssim 17$, covered by the bulk of our objects. It is important, however, to compare our proper motions with those from other catalogues because their proper motions may be preferable for the brightest stars or for a rare case where the GSC-II + SDSS DR7 error is unusually large.

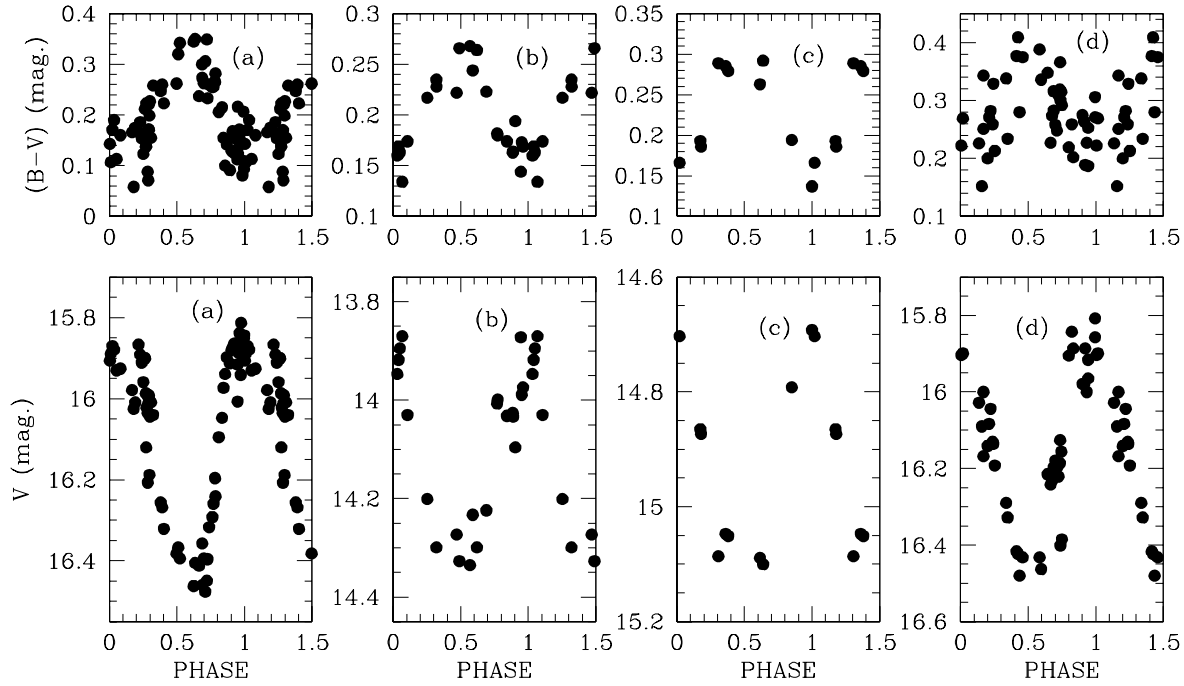


Figure B2. The V and $(B - V)$ light curves for the RR Lyrae variable: (a) RR7-101, (b) AF-400, (c) AF-430 and (d) RR7-086. Further information on these stars is given in Table B1.

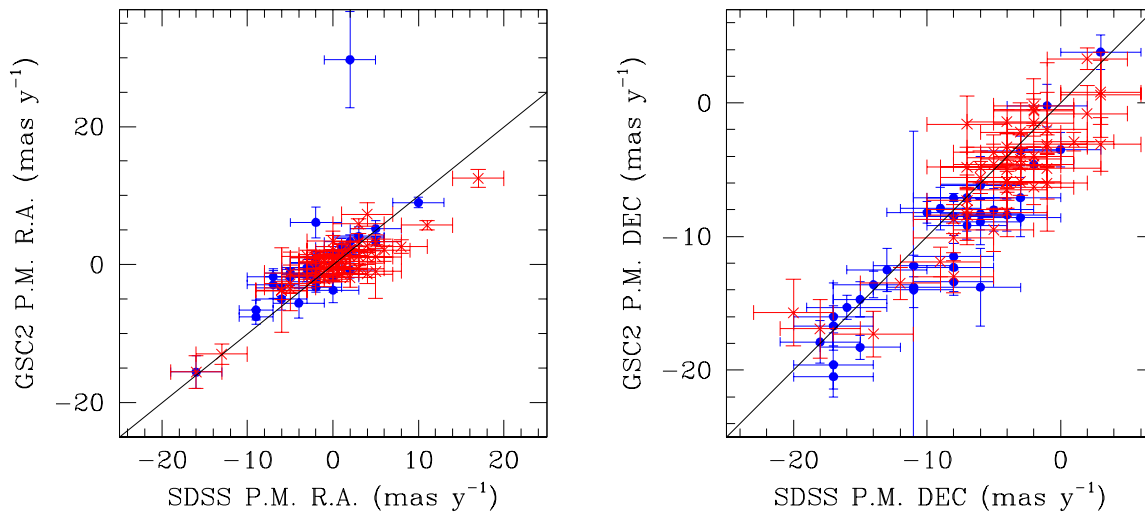


Figure C1. A comparison between the GSCII-SDSS proper motions (ordinate) and those given in the SDSS DR7 catalogue (abscissa). The plot on the left is for proper motions in R.A. and that on the right is for proper motions in Declination. The units are milliarcseconds per year. The proper motions of the BHB stars are shown by blue filled circles and those of the RR Lyrae stars by red crosses.

C1 Proper Motions for the Brighter or Anomalous Stars.

Table C1 gives the GSCII—SDSS proper motions for our brighter program stars together with those given by the NOMAD catalogue (Zacharias et al., 2004), the UCAC3 catalogue (Zacharias et al., 2009) and the SDSS DR7 catalogue (Abazajian et al., 2009). Fol-

lowing this comparison, we have chosen to use the NOMAD proper motions for the brighter BHB stars RR7-15, RR7-64, BS 16473-09 and BS 16927-22 and for the brighter RR Lyrae stars TT Lyn, X

LMi and DQ LYN⁸. These are all stars whose V magnitudes are brighter than 12.3

Fig C1 gives separate plots for the proper motions in R.A. and Declination for the GSC-II—SDSS against those given by the SDSS DR7. Both catalogues are based on quite similar material (i.e. first epochs from the POSS photographic plates and second epochs from the SDSS measurements), but they were processed and calibrated in different and independent ways. The plot shows good agreement in general at the milliarc second per year level except for the proper motion in R.A. for the BHB star P 30-38. We have preferred the SDSS DR7 proper motion because it roughly agrees with that given by the NOMAD catalogue and because the errors in the GSC-II—SDSS catalogue for this star are unusually large.

APPENDIX D: THICK DISC

Fig. D1 shows the L_{\perp} vs L_z plot for the thick disc stars within 2 kpc from Bensby et al. (2011) (crosses) and the thick disc stars within 0.5 kpc (Ages 8 to 11 Gyr and $-0.4 < [\text{Fe}/\text{H}] < -0.5$) from the Geneva-Copenhagen Survey of the Solar Neighbourhood III (Holmberg et al., 2009) (small black open circles); Most of these stars have $L_{\perp} < 650$ kpc km s⁻¹ and $1100 < L_z < 2000$ kpc km s⁻¹; we have used these limits to define the location of stars that belong to the thick disc.⁹ There is a strong concentration of local RR Lyrae stars (red circles) in this location but rather few local BHB stars (Fig D1); these stars are listed in Table D1. Table D2 gives the mean properties of the 46 RR Lyrae stars in this thick disc location: 5 stars (11%) have $[\text{Fe}/\text{H}] \leq -1.50$ and have a high probability of being *halo* stars; 19 (41%) have $[\text{Fe}/\text{H}] > -0.5$ and can definitely be called *disc* stars. The remaining 22 (48%) have intermediate $[\text{Fe}/\text{H}]$ ($-0.5 > [\text{Fe}/\text{H}] > -1.5$) and mean values of their orbital eccentricity and maximum orbital height above the galactic plane (z_{max}) and angular momentum L_{\perp} that lie between those of the stars with $[\text{Fe}/\text{H}] > -0.5$ and those with $[\text{Fe}/\text{H}] < -1.5$. All of the 19 RR Lyrae stars with $[\text{Fe}/\text{H}] > -0.7$ and 73% of the 22 with $-0.7 > [\text{Fe}/\text{H}] > -1.5$ have $L_{\perp} < 325$ kpc km s⁻¹; consequently ~82% of the likely thick disc stars, those with $[\text{Fe}/\text{H}] > -1.5$, should have $L_{\perp} < 325$ kpc km s⁻¹ and $1100 < L_z < 2000$ kpc km s⁻¹. The isolation of a purer sample of disc stars requires additional chemical or kinematic information. Only three local BHB stars (within 1 kpc) have $L_{\perp} < 650$ kpc km s⁻¹ and $1100 < L_z < 2000$ kpc km s⁻¹ and two of these have $[\text{Fe}/\text{H}] < -2.0$ and so are almost certainly *halo* stars. Thus, unlike RR Lyrae stars, BHB stars do not have a strong *disc* component in the solar neighbourhood as was found by Kinman et al. (2009).

APPENDIX E: THE ANGLAR MOMENTA L_{\perp} AND L_z FOR OBJECTS IN FIGURES 4, 5 & 6.

Tables E1, E2, E3 & E4 give the Anglar Momenta L_{\perp} and L_z for the RR Lyrae stars at the North Galactic Pole (Table 2 in Kinman et al., 2007b), the BHB stars at the North Galactic Pole (Table 1 in Kinman et al., 2007b), Local BHB stars within 1 kpc (Kinman et al., 2000) using proper motions taken from the NOMAD catalogue (Zacharias et al., 2009) and Globular Clusters within 10 kpc. We have only included RR Lyrae and BHB stars at the North Galactic Pole whose distances are less than 10 kpc.

Definitions of L_{\perp} and L_z are given in the Appendix of Kepley et al. (2007). The calculations of these quantities and their errors were made using a program kindly made available by Heather Morrison and modified for our use by Carla Cacciari. Table E5 compares the values of L_{\perp} and L_z that we calculated with this program for a number of halo objects with those given by Re Fiorentin et al. (2005) and Morrison et al. (2009). The differences are generally less than the quoted errors and are probably largely produced by differences in the proper motions that were used. An exception is HD 128279, where our values of L_{\perp} and L_z agree with those of Re Fiorentin et al. (2005) but not with those of Morrison et al. (2009).

⁸ The NOMAD catalogue was chosen because the proper motion that it gives for a given object is the one which is preferred from among a number of major catalogues (all of which are on the International Celestial Reference System).

⁹ Only one disc RR Lyrae (TW Lyn) is known to lie outside this location

[h]

Table C1. A Comparison of the proper motions from different sources for the brightest of our program stars.

Star	$\langle V \rangle$ (mag)	SDSS (DR7)		NOMAD		UCAC3		GSCII-SDSS	
		μ_α mas y ⁻¹	μ_{dec} mas y ⁻¹	μ_α mas y ⁻¹	μ_{dec} mas y ⁻¹	μ_α mas y ⁻¹	μ_{dec} mas y ⁻¹	μ_α mas y ⁻¹	μ_{dec} mas y ⁻¹
RR7-15	11.75	-20.2±1.0	-35.0±0.7	-19.1±2.0	-36.0±0.8	-12.0±3.0	-43.5±1.7
RR7-23	12.63	+07.7±1.6	-22.6±0.7	+07.6±1.3	-22.0±0.6	+09.6±1.7	-25.0±1.4
RR7-64	11.23	-05.1±0.7	-05.4±0.7	-06.0±1.6	-05.0±1.0	-02.4±2.9	-00.2±1.6
11419-01	12.79	-02±3	-15±3	-08.0±1.0	-20.1±0.7	-08.3±3.1	-17.5±1.4	+06.1±2.2	-18.3±0.9
16473-09	10.91	-01.7±0.6	-00.1±0.7	-02.2±0.9	-00.3±0.6	+10.7±3.1	-17.9±5.5
P 30-38	14.39	+02±3	-11±3	+04.1±5.9	-11.7±5.6	+29.7±7.0	-14.0±11.9
16927-22	11.18	+06.8±0.8	-29.8±0.6	+06.0±0.9	-30.3±0.7	+09.2±0.6	-30.0±1.2
RW LYN	12.91	+03±3	-18±3	+06.3±0.7	-23.4±1.2	+07.5±1.0	-23.6±0.8	+07.3±1.7	-15.7±2.5
TT LYN	09.84	-81.9±1.5	-41.8±0.9	-84.6±0.8	-42.4±0.7	-50.2±13.6	-25.6±9.2
TW LYN	12.07	-06.6±5.0	-01.1±3.2	+03.2±0.8	+04.3±0.7	+00.6±3.8	+02.6±2.9
X LMi	12.30	+07.8±1.3	-17.3±0.7	+06.6±1.0	-16.7±1.0	+12.4±3.2	-14.0±5.1
DQ LYN	11.46	-01.9±0.8	-28.7±1.0	-01.0±1.0	-29.7±2.7	+02.9±1.8	-20.5±2.8
RR7-079	13.44	-02±3	-12±3	-15.5±3.8	-18.7±3.6	-17.8±4.3	-18.9±4.1	+01.0±1.1	-13.5±1.2

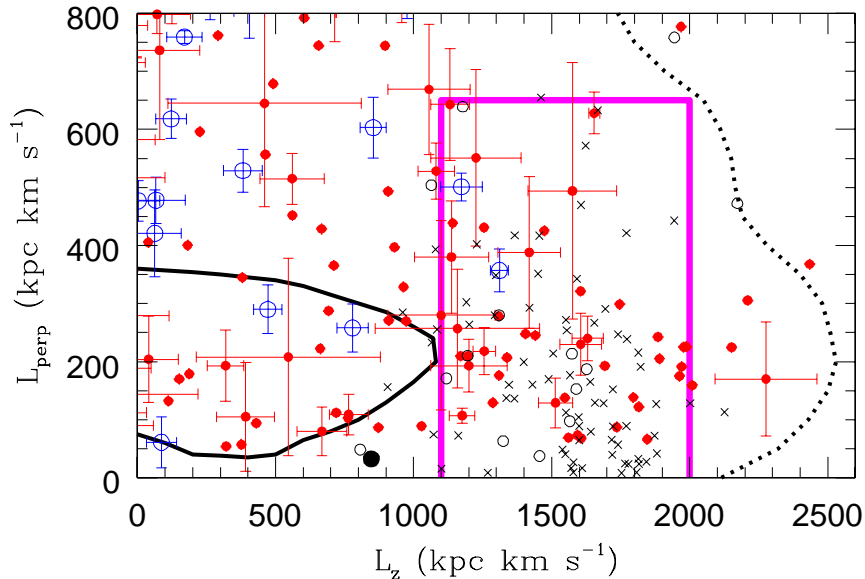


Figure D1. Angular Momenta L_\perp vs L_z . RR Lyrae stars within 1 kpc are shown by red filled circles. Open circles are stars within 500 pc, Age 8 to 11 Gyr, $-0.4 > [\text{Fe}/\text{H}] > -0.5$ taken from the Geneva - Copenhagen Survey (Holmberg et al., 2009). Crosses are thick disc stars within 2 kpc taken from Bensby et al. (2011). The large black filled circle is the star Arcturus. The black full and dotted contours are taken from Fig 3 of Morrison et al. (2009). The magenta box shows the adopted location of the Thick Disc stars.

APPENDIX F: GROUPS OF OUTLIERS.

This section summarizes additional data about the two groups of outliers called H99 and K07.

F1 The H99 group.

This group was discovered by Helmi et al. (1999) and further investigated by Re Fiorentin et al. (2005). Roederer et al. (2010) made a detailed chemical analysis of these stars (excluding the RR Lyrae stars) and showed that they had a metallicity range of

$-3.4 < [\text{Fe}/\text{H}] < -1.5$ but were otherwise chemically homogeneous. They concluded that the wide metallicity range precluded the progenitor being a single globular cluster. We note that the globular cluster NGC 6205 (M13) ($[\text{Fe}/\text{H}] = -1.57$) has a rather similar L_\perp to that of this group but a different L_z . The 4 RR Lyrae stars that belong to the H99 group RZ CEP, TT CNC, AR SER and TT LYN have $[\text{Fe}/\text{H}] = -1.77, -1.57, -1.78$ and -1.56 respectively (Re Fiorentin et al. 2005), and XZ CYG and CS ERI have $[\text{Fe}/\text{H}] = -1.44$ and -1.41 respectively. The mean $[\text{Fe}/\text{H}]$ of these six RR Lyrae stars is -1.59 and the *rms* scatter in their $[\text{Fe}/\text{H}]$ about this mean is 0.16 which is comparable with the likely error in their metallic-

Table D1. Candidates for Thick Disc RR Lyrae and BHB stars with distances (D) within 2 kpc.

D < 1 kpc							1 < D < 2 kpc						
Star	[Fe/H]	S [†]	Ecc.	z_{max}	L_{\perp}	L_z	Star	[Fe/H]	S [†]	Ecc.	z_{max}	L_{\perp}	L_z
RR LYRAE:							RR LYRAE:						
FW LUP	-0.20	(1)	0.06	0.13	068	1607	CN LYR	-0.58	(1)	0.16	0.32	66	1846
KX LYR	-0.46	(2)	0.31	0.41	069	1561	CG PEG	-0.50	(1)	0.03	0.39	87	1736
DX DEL	-0.50	(1)	0.22	0.23	073	1594	HH PUP	-0.50	(1)	0.12	0.35	122	1815
SW DRA	-1.12	(1)	0.42	0.71	107	1176	ST OPH	-1.30	(2)	0.10	0.56	129	1514
AV PEG	-0.36	(1)	0.27	0.39	129	1287	TW HER	-0.88	(1)	0.13	0.61	139	1796
v494 SCO	-1.01	(2)	0.12	0.21	138	1548	SS CNC	-0.56	(1)	0.18	0.83	159	2009
RS BOO	-0.62	(1)	0.17	0.94	191	1971	TW LYN	-0.66	(1)	0.21	2.13	170	2276
SW AND	-0.41	(1)	0.13	0.47	193	1692	TZ AQR	-1.24	(1)	0.20	1.39	193	1200
DH PEG	-1.24	(2)	0.27	0.52	207	1338	Z MIC	-1.10	(1)	0.39	1.25	210	1196
AR PER	-0.57	(1)	0.06	0.40	226	1987	UW OCT	-0.49	(2)	0.47	1.58	210	1170
UY CYG	-0.95	(1)	0.11	0.23	240	1630	EZ LYR	-1.29	(1)	0.42	0.65	176	1309
AN SER	-0.39	(1)	0.10	0.84	245	1440	RR LEO	-1.51	(1)	0.38	1.04	218	1256
v690 SCO	-1.16	(2)	0.19	0.48	248	1405	RR GEM	-0.55	(1)	0.18	0.73	225	2152
DM CYG	-0.57	(1)	0.13	0.48	205	1890	AA CMI	-0.15	(1)	0.09	0.43	225	1978
XZ DRA	-0.89	(1)	0.10	0.68	299	1746	AV SER	-1.20	(3)	0.11	0.86	230	1605
v445 OPH	-0.19	(2)	0.11	0.81	388	1419	RW ARI	-1.16	(2)	0.26	1.44	238	1639
T SEX	-1.33	(1)	0.30	1.18	431	1255	U PIC	-0.72	(1)	0.09	1.01	242	1885
UU VIR	-0.87	(2)	0.52	1.71	439	1142	BS APS	-1.33	(2)	0.30	1.12	264	1852
RX ERI	-1.33	(1)	0.00	1.67	628	1654	CP AQR	-0.77	(1)	0.31	1.07	278	1308
W CVN	-1.22	(1)	0.29	2.47	643	1132	RW DRA	-1.55	(2)	0.60	1.11	280	1100
							RW TRA	-0.13	(1)	0.14	0.78	321	1605
							AT SER	-2.03	(1)	0.16	1.47	380	1137
BHB:							BR AQR	-0.74	(1)	0.11	1.65	426	1473
HD 4850	-1.18	(4)	357	1311	VV PEG	-1.88	(2)	0.26	2.55	495	1575
HD 8376	-2.82	(4)	501	1173	RV SEX	-1.10	(2)	0.40	2.14	551	1226
BD +01 0548	-2.23	(4)	299	1794	BO AQR	-1.80	(2)	0.46	1.82	257	1159

[†] Sources of [Fe/H]: (1) Feast et al. (2008); (2) Beers et al. (2000); (3) Layden et al. (1994); (4) Kinman et al. (2009).

The orbital eccentricity (Ecc.) and the maximum height in kpc above the galactic plane (z_{max}) are taken from Maintz & de Boer (2005). L_{\perp} and L_z are in units of kpc km s^{-1} .

Table D2. Mean properties of RR Lyrae stars with $1100 < L_z < 2000 \text{ kpc km s}^{-1}$ and $L_{\perp} \text{ kpc km s}^{-1}$ as a function of [Fe/H].

Range in [Fe/H]	Number of stars	$\langle [\text{Fe}/\text{H}] \rangle$	$\langle \text{Ecc.} \rangle$	$\langle z_{max} \rangle$ kpc	$\langle J_{\perp} \rangle$ $\text{km s}^{-1} \text{ kpc}$
$[\text{Fe}/\text{H}] \leq -1.50$	5	-1.75 ± 0.11	0.37 ± 0.09	1.60 ± 0.31	326 ± 56
$-0.70 \leq [\text{Fe}/\text{H}] < -1.50$	22	-1.09 ± 0.04	0.23 ± 0.03	1.07 ± 0.13	293 ± 36
$[\text{Fe}/\text{H}] \geq -0.70$	19	-0.44 ± 0.04	0.17 ± 0.02	0.67 ± 0.11	177 ± 21

The orbital eccentricity (Ecc.) and the maximum height in kpc above the galactic plane (z_{max}) are taken from Maintz & de Boer (2005)

Table E1. Angular Momenta L_{\perp} and L_z for RR Lyrae stars at the North Galactic Pole[†].

Star	L_{\perp}	L_z	Star	L_{\perp}	L_z	Star	L_{\perp}	L_z
NSV5476	1074 ± 440	-1005 ± 497	SV-CVn	1059 ± 228	-0827 ± 238	IP-Com	1878 ± 780	-1860 ± 780
V-Com	1001 ± 454	$+0902 \pm 1285$	FV-Com	0786 ± 369	$+0611 \pm 497$	SA57-019	1041 ± 389	-1089 ± 438
CD-Com	6464 ± 768	-4461 ± 795	U-Com	0690 ± 057	-0723 ± 160	EO-Com	1743 ± 483	-1889 ± 528
AF-031	3935 ± 710	-2075 ± 1170	SW-CVn	0469 ± 210	$+0153 \pm 313$	TZ-CVn	0903 ± 368	-1010 ± 595
TU-Com	0951 ± 628	-1218 ± 1459	DV-Com	1406 ± 595	-0718 ± 721	SA57-047	2809 ± 515	-3615 ± 516
CK-Com	2207 ± 407	-2985 ± 459	AF-791	4599 ± 544	$+1355 \pm 442$	MQ-Com	1572 ± 393	-1895 ± 501
CL-Com	0868 ± 592	$+0165 \pm 476$	TX-Com	1101 ± 405	-0993 ± 395	IS-Com	1472 ± 177	-1642 ± 338
AT-CVn	1103 ± 666	-0409 ± 1106	AP-CVn	0875 ± 419	-0254 ± 359	AF-882	0636 ± 315	-0445 ± 390
RR-CVn	0465 ± 118	-1375 ± 336	AF-155	1078 ± 548	-0310 ± 739			
S-Com	0560 ± 083	$+0147 \pm 260$	TY-CVn	0802 ± 263	-0747 ± 471			

[†] The stars are identified in Table 2 of Kinman et al. (2007b); L_{\perp} and L_z are in units of kpc km s^{-1} .

Table E2. Angular Momenta L_{\perp} and L_z for BHB stars at the North Galactic Pole[†].

Star	L_{\perp}	L_z	Star	L_{\perp}	L_z	Star	L_{\perp}	L_z
16549-51	0605±363	-0197±234	AF-078	0990±209	+1159±314	SA57-001	1430±342	-1742±503
AF-006	0499±164	-0973±349	AF-769	0646±189	-1423±408	SA57-006	0404±191	-0280±412
AF-727	0916±159	+1812±323	16026-67	0523±153	-0946±443	SA57-007	0590±343	-0135±215
AF-729	1193±577	-1024±717	AF-100	0410±149	-0656±325	SA57-017	0810±253	-1037±492
AF-029	1080±450	+1127±591	16466-08	0742±480	-0298±555	SA57-032	1621±604	-1514±670
AF-030	0800±392	-0902±514	AF-108	1279±224	-2185±370	SA57-040	0794±320	+0719±358
16022-26	0708±350	-0574±571	AF-111	1796±308	+1059±394	SA57-045	1025±405	+0035±379
AF-038	2494±824	-1878±1130	AF-112	0509±091	+1126±180	AF-825	1082±407	+0263±247
AF-041	1668±511	-1928±635	AF-113	0284±067	-0940±159	AF-841	0303±157	-391±273
AF-045	0555±075	+1342±180	AF-115	1571±457	-1484±494	AF-848	0716±085	+0648±176
AF-048	0230±123	+0118±314	16466-15	1220±154	+1194±453	SA57-066	1856±420	+0428±601
AF-052	1583±776	-0621±785	AF-131	1329±612	-0759±664	AF-854	1820±584	-0275±456
AF-053	2091±768	-1609±828	AF-134	0688±117	+0211±155	SA57-080	0555±229	+0244±366
16026-28	0746±094	+1411±179	16031-44	0913±182	+0163±457	AF-866	0458±281	-0132±396
AF-754	1161±733	-0175±1120	15622-48	0502±276	-0436±507	AF-900	1052±378	+0069±203
AF-755	1582±762	-0676±1068	15622-07	0224±105	+0417±322	AF-909	0534±249	+0144±330
AF-068	1160±405	+0257±460	AF-138	1113±299	-0837±494	AF-914	1054±394	-0232±304
AF-070	1037±400	-0050±570	15622-09	0652±113	+0379±262	AF-916	0772±284	+0803±274
AF-075	2398±809	-1208±760	AF-797	1318±417	-1194±519	AF-918	0439±247	+0261±318
AF-076	1741±720	-0524±599	AF-804	0397±153	-0258±312			

[†] The stars are identified in Table 1 of Kinman et al. (2007b); L_{\perp} and L_z are in units of kpc km s⁻¹.

Table E3. Angular Momenta L_{\perp} and L_z for Local BHB stars[†].

Star	L_{\perp}	L_z	Star	L_{\perp}	L_z	Star	L_{\perp}	L_z
HD 2857	0421±075	+0063±098	HD 78913	0172±038	-0769±040	HD117880	0319±108	-0701±168
HD 4850	0357±037	+1311±032	HD 86968	0477±035	+0003±078	HD 128801	0828±037	+0977±038
HD 8376	0501±024	+1173±75	HD 87047	1124±037	-0738±131	HD 130095	0579±031	-0184±167
HD 13780	0258±041	+0779±057	HD 87112	0399±48	-0316±099	HD 130201	0603±052	+0854±47
HD 14829	1215±045	+0272±104	HD 93329	0599±048	-0814±078	HD 139961	0766±039	-1211±162
HD 31943	0290±042	+0472±052	HD 106304	1305±064	-0009±052	HD 161817	1033±018	-0530±029
HD 252940	0529±037	+0382±070	BD +42° 2602	0835±046	+0263±110	HD 167105	0061±044	+0087±054
HD 60778	0888±051	+0638±053	HD 109995	0759±011	+0170±064	HD 180903	0618±034	+0122±055
HD 74721	0803±046	+0405±055	BD +25° 2602	0478±040	+0067±107	HD 213468	1282±040	-0119±189

[†] The stars are taken from Table 1 of Kinman et al. (2000); L_{\perp} and L_z are in units of kpc km s⁻¹.

ity. The period distribution of the six RR Lyrae stars correspond to Oosterhoff type I; NGC 6205 has too few RR Lyrae stars to have a reliable Oosterhoff type. The RR Lyrae members of H99 therefore are more homogeneous than the later-type stars in the group and could possibly have originated from a single globular cluster.

F2 The K07 group.

Kepley et al. (2007) identified six low metallicity *outliers* in their Table 5. Two of these *outliers* (RV CAP and HD 214925) that have similar location on the L_{\perp} vs L_z plot and 13 other *outliers* are also close to this location. The assumed boundaries of what we call the K07 group are $-2300 < L_z < -1500$ and $+1300 < L_{\perp} < +2200$ and are shown by the green rectangle in Figs. 4, 5 & 6. The 15 low metallicity stars within these boundaries are listed in Table 3. These stars cover a wide range of distances and it seems unlikely that they all belong to the same group. It is more likely that they belong to several groups that have similar L_{\perp} and L_z . Thus, AT VIR and RV CAP (at ~ 1 kpc) have similar properties and IP COM and EO COM (at ~ 7 kpc) also have similar properties. Further analysis requires more accurate data and is beyond the scope of this paper.

Table E4. Angular Momenta L_{\perp} and L_z for Galactic Globular Clusters within 10 kpc[†].

Cluster	L_{\perp}	L_z	Cluster	L_{\perp}	L_z	Cluster	L_{\perp}	L_z
NGC 104	0618±064	+1169±051	NBC 6093	0299±127	-0005±053	NGC 6522	0199±079	+0057±215
NGC 288	0571±075	-0244±109	NGC 6121	0073±024	+0136±074	NGC 6553	0154±018	+0920±180
NGC 362	0377±146	-0225±132	NGC 6144	0379±026	-0179±013	NGC 6626	0145±031	+0480±113
NGC 3201	1199±086	-2659±098	NGC 6171	0358±065	+0367±111	NGC 6656	0521±092	+0843±114
NGC 4372	0596±095	+0813±054	NGC 6205	2066±258	-0446±194	NGC 6712	0383±054	+0109±125
NGC 4833	0197±064	+0174±116	NGC 6218	0334±034	+0758±074	NGC 6723	0437±056	-0045±112
NGC 5139	0114±023	-0439±020	NGC 6254	0557±061	+0630±106	NGC 6752	0336±018	+0971±068
NGC 5272	1255±224	+0644±180	NGC 6266	0178±022	+0231±102	NGC 6809	0759±040	+0134±075
NGC 5904	1198±317	+0337±091	NGC 6304	0093±009	+0338±101	NGC 6838	0097±047	+1161±020
NGC 5927	0225±065	+1028±051	NGC 6397	0764±022	+0503±043	NGC 7009	0715±114	-0457±110

[†] L_{\perp} and L_z are in units of kpc km s⁻¹. They were derived from the data given by Vande Putte & Cropper (2009).

Table E5. Comparison of Angular Momenta L_{\perp} and L_z for Halo stars derived from three sources[†].

Star	<i>This Paper</i>		<i>Morrison et al.(2009)</i>		<i>Re Fiorentin et al. (2005)</i>	
	L_{\perp}	L_z	L_{\perp}	L_z	L_{\perp}	L_z
UY CYG	0113±048	+1670±061	0240±038	+1630±057
VZ HER	0196±072	+0316±075	0193±061	+0319±066
RV SEX	0421±131	+1279±199	0551±152	+1226±164
SW BOO	0686±097	-0022±155	0878±175	+0616±394
AN LEO	1232±123	-0201±250	1014±234	+0220±372
V LMI	0377±116	+0142±154	0208±170	+0546±334
X LMI	0223±064	+1005±080	0255±176	+0913±329
UV VIR	0356±130	-0510±196	0144±126	-0070±290
TT CNC	2027±238	+0797±128	2123±225	+0718±119	2483±...	+0562±...
AR SER	2082±135	+0656±196	2017±108	+0637±170	1934±...	+0322±...
TT LYN	1959±129	+0838±074	2032±136	+0847±072	2124±...	+0748±...
HD 128279	2075±320	+1046±188	0475±050	+2220±030	1844±...	+1194±...
HD 237846	1546±032	+0931±038	1568±026	+0948±033	1443±...	+0774±...
HD 214161	2181±075	+0941±064	2125±087	+0836±134	2173±...	+0952±...

[†] L_{\perp} and L_z are in units of kpc km s⁻¹.

REFERENCES

- Abazajian, K., Adelman-McCarthy, J., Agüeros, M. et al., 2009, ApJS, 182, 543 (SDSS Data Release 7)
- AN, D., Johnson J., Clem, J., Yanny, B., Rockosi, C., et al. 2008, ApJS, 179, 326
- Andrei, A., Souchay, J., Zacharias, N., Smart, R., et al., 2009, A&A, 505, 385
- Beers, T.C., Wilhelm, R., Dionidis, S.P. & Mattson, C.J. 1996, ApJ Suppl., 103, 433
- Beers, T.C., Chiba, M., Yoshii, Y. et al. 2000, AJ, 119, 2866
- Beers, T., Carollo, D., Ivezić, D., An, D., et al. 2012, ApJ, 746, 34
- Behr, B., 2003, ApJS, 149, 101
- Bell, E., Xue, X., Rix, H-W., Ruhland, C., Hogg, D. 2010, AJ, 140, 1850
- Benedict, G.F., McArthur, B., Feast, M., Barnes, T., Harrison, T. et al. 2011, AJ, 142, 187
- R Bensby, T., Alves-Brito, A., Oey, M., Yong, D., Meléndez, J., 2011, ApJL, 735, 46
- Brown, W.R., Geller, M.J., Kenyon, S.J. et al. 2003, AJ, 126, 1362
- Brunthaler, A., Reid, M., Menten, K., Zheng, X.-W., Bartkiewicz, A., Choi, Y. et al., 2011, AN, 332, 461
- Cacciari, C., Corwin, T., Carney, B., 2005, AJ, 129, 267
- Cardelli, J.A., Clayton, G.C. & Mathis, J.S. 1989, ApJ, 345, 245
- Carollo, D., Beers, T., Lee, Y., Chiba, M., et al., 2007. Nature, 450, 1020
- Carollo, D. Beers, T., Chiba, M., Norris, J. et al., 2010, ApJ, 712, 692
- Carollo, D. Beers, T., Bovy, J., Sivarani, T. et al., 2012, ApJ, 744, 195
- Chiba, M., Beers, T. C. 2000, AJ, 119, 2843
- Clement, C., Muzzin, A., Dufton, Q., Ponnampalam, T., Wang, J., Burford, J., et al., 2001, AJ, 122, 2587
- Clementini, G., Gratton, R., Bragaglia, A., Carretta, E., Di Fabrizio, L. & Maio, M. 2003, AJ, 125, 1309
- De Jong, J., Yanny, B., Rix, H.-W., Dolphin, A. et al., 2010, ApJ, 714, 663
- De Lee, N., 2008, PhD Thesis, Michigan State University, Lansing, Michigan, U.S.A.
- Deason, A., Belokurov, V., Evans, N., 2011, MNRAS, 416, 2903
- Dehnen, W., Binney, J. J. 1998, MNRAS, 298, 387
- Dorman, B., Rood, R., O'Connell, R., 1993, ApJ, 419, 596
- Dotter, A., Sarajedini, A., Anderson, J., Aparicio, A., et al. 2010, ApJ, 708, 698
- Feast, M., Laney, C., Kinman, T., van Leeuwen, F., Whitelock, P., 2008, MNRAS, 386, 2115
- Feast, M. 2011, Carnegie Observatories Astrophysics Series, Vol. 5, ed. A. McWilliam (Pasadena: Carnegie Observatories)
- Fernley, J., Barnes, T. 1997, A&AS, 125, 313
- Ferraro, F.R., Carretta, E., Corsi, C.E., Fusi Pecci, F., Cacciari, C., Buonanno, R., Paltrinieri, B. & Hamilton, D. 1997, A & A, 320, 757
- Font, A., McCarthy, I., Crain, R., Theuns, T., et al., 2011, MNRAS, 416, 2802
- Hattori, K., Yoshii, Y., 2011, MNRAS, 418, 2418
- Helmi, A., White, S.D., de Zeeuw, P.T. & Zhao, H. 1999, Nature, 402, 53
- Helmi, A. 2008, Astron. Astrophys. Rev. 15, 145
- Holmberg, J., Nordström, B., Andersen, J., 2009, A&A, 501, 941
- Jeffery, E., Barnes, T., Skillen, I., Montemayor, T., 2007, ApJS, 171, 512
- Johnson, D. R. H., Soderblom, D. R. 1987, AJ, 93, 864
- Jones, B.F. & Walker, M.F. 1988, AJ, 95, 1755
- Jurcsik, J., Kovacs, G., 1996, A&A, 312, 111
- Jurcsik, J., Sodor, A., Varadi, M., Vida, K., Posztobanyi, K., Szing, A., et al., IBVS, 5709
- Kemper, E., AJ, 87, 1395
- Kepley, A. Morrison, H. Helmi, A., Kinman, T. et al. 2007, AJ, 134, 1579
- Kholopov, P. et al. 1985 Gen. Cat. of Variable Stars (<http://www.sai.msu.ru/gcvs/gcvs/>)
- Kinemuchi, K., Smith, H., Woźniak, P., McKay, T., 2006, AJ, 132, 1202
- Kinman, T., Wirtanen, C., Janes, K., 1966, ApJS, 13, 379
- Kinman, T., Mahaffey, C., Wirtanen, C., 1982, AJ, 87, 314
- Kinman, T.D., Suntzeff, N.B., Kraft, R.P., 1994, AJ, 108, 1722
- Kinman, T. D., Castelli, F., Cacciari, C., Bragaglia, A., Harmer, D., Valdes, F., 2000, A&A, 364, 102
- Kinman, T., Saha, A., Pier, J., 2004, ApJL, 605, 25
- Kinman, T., Salim, S., Clewley, L., 2007a, ApJL, 662, 111
- Kinman, T., Cacciari, C., Bragaglia, A., Buzzoni, A., Spagna, A. 2007b, MNRAS, 375, 1381
- Kinman, T., Morrison, H., Brown, W., 2009, AJ, 137, 3198
- Kinman T. Brown, W., 2010, IBVS 5935
- Kinman T. Brown, W., 2011, AJ, 141, 168
- Klement, R.J., 2010, Astron. Astrophys. Rev., 18, 567
- Lasker, B.M., Lattanzi, M., McLean, B., et al. 2008, AJ, 136, 735
- Layden, A. 1994, AJ, 108, 1016
- Lee, J-W., Carney, B.W. 1999, AJ, 118, 1373
- Liu, T., Janes, K., 1990, ApJ, 354, 273
- Maintz, G., 2005, A&A, 442, 381
- Maintz, G. & de Boer, K.S. 2005, A&A, 442, 229
- Marín-Franch, A., Aparicio, A., Piotto, G., Rosenberg, A., et al., 2009, ApJ, 694, 1498
- McCarthy, I., Font, A., Crain, R., Schaye, J. et al., 2012, MNRAS, in press
- McClusky, J. 2008, IBVS 5825
- Miceli, A., Rest, A., Stubbs, C., Hawley, S., et al., 2008, ApJ, 678, 865
- Morrison, H., Helmi, A., Sun, J., Liu, P., et al. 2009, ApJ, 694, 130
- Nemec, J., Nemec, A., Lutz, T., 1994, AJ, 108, 222
- Oser, L., Ostriker, J., Naab, T., Johansson, P. et al., 2010, ApJ., 725, 2312
- Paltrinieri, B., Ferraro, F.R., Fusi Pecci, F. & Carretta, E. 1998, MNRAS, 293, 434
- Pesch, P., Sanduleak, N. 1989, ApJS, 71, 549
- Pier, J., Saha, A., Kinman, T., 2003, IBVS 5459
- Preston, G. W., Shectman, S. A., Beers, T. C. 1991, ApJ, 375, 121
- Re Fiorentin, P., Helmi, A., Lattanzi, M., Spagna, A., 2005, A&A, 439, 551
- Reid, M., Brunthaler, 2004, ApJ, 616, 872
- Roederer, I., Sneden, C., Thompson, I., Preston, G., Shectman, S., 2010, ApJ, 711, 573
- Ruhland, C., Bell, E., Rix, H-W., Xue, X., 2011, ApJ, 731, 119
- Saha, A., Oke, B., 1984, ApJ, 285, 688
- Schlegel, D. J., Finkbeiner, D. P., Davis, M. 1998, ApJ, 500, 525
- Schmidt, M., 1956, B.A.N. 13, 15
- Schmidt, E., 2002, AJ, 123, 965
- Schmidt, E., Chab, J. Reiswig, D., 109, 1239
- Schmidt, E., Seth, A., 1995, AJ, 112, 2769
- Schönrich, R., Asplund, M., Casagrande, L., 2011, MNRAS, 415, 3807

- Sesar, B., Ivezić, Z., Grammer, S., Morgan, D., et al., 2010, ApJ, 708, 717
- Sesar, B., Jurić, M., Ivezić, Ž., 2011, ApJ, 731, 4
- Sirko, E., Goodman, J., Knapp, G.R. et al. 2004, AJ, 127, 899
- Smith, M., Evans, N., Belokurov, V., Hewitt, P., et al., 2009, MNRAS, 399, 1223
- Smith, K., Bailer-Jones, C., Klement, R., Xue, X. 2010, A&A, 522, 88
- Smith, H., Catelan, M., Kuehn, C. 2011, Carnegie Obs. Astrophysics Ser., Vol. 5 (ed. A. McWilliam) (Pasadena: Carnegie Obs.)
- Sodor, A., Jurcsik, J., Szeidl, B., 2009, MNRAS, 394, 261
- Spagna, A., Bucciarelli, B., Lattanzi, M., Re Fiorentin, P., Smart, R., 2010a, Mem. S.A. It., 14, 67
- Spagna, A., Lattanzi, M., Re Fiorentin, P., Smart, R., 2010b, A&A, 510, L4
- Usher, P., Mitchell, K. 1982, ApJS, 49, 27
- Valenti, E., Ferraro, F.R., Perina, S. & Origlia, L. 2004, A&A, 419, 139
- van den Bergh, S. 1993, AJ, 105, 971
- Vande Putte, D., Cropper, M., 2009, MNRAS, 392, 113
- Watkins, L., Evans, N., Belokurov, V., Smith, M., et al., 2009, MNRAS, 398, 1757
- Xue, X.X., Rix, H.-W., Yanny, B., Beers, T. et al. 2011. ApJ, 738, 79
- Yanny, B., Rockosi, C., Newberg, et al. 2009, AJ, 137, 4377
- Zacharias, N., Monet, D., Levine, S., et al. 2004, BAAS, 36, 1418 (NOMAD Catalogue)
- Zacharias, N., Finch, C., Girard, T., Hambly, N. et al., 2009, AJ, 139, 2184 (UCAC3 Catalogue)
- Zinn, R. 1993, in *The Globular Cluster – Galaxy Connection*, eds. Smith, G & Brodie, J., ASP Conf. Ser. Vol. 48, p. 38
- Zolotov, A., Willman, B., Brooks, A., Governato, F. et al. 2009, ApJ, 721, 738
- Zolotov, A., Willman, B., Brooks, A., Governato, F. et al. 2010, ApJ, 738, 79
- Zolotov, A., 2011, BAAS, 43, 2011.